Science
AAAS

Supplementary Materials for

A shift in the mechanisms controlling hippocampal engram formation during brain maturation

Adam I. Ramsaran *et al*.

Corresponding author: Paul W. Frankland, paul.frankland@sickkids.ca

Science **380**, 543 (2023)
DOI: 10.1126/science.ade6530

The PDF file includes:

Other Supplementary Material for this manuscript includes the following:

Materials and Methods

Mice

Two mouse lines were used. Male and female F1 hybrid (C57BL/6NTac x 129S6/SvEvTac) wild-type (WT) mice were used for all experiments, except where noted. Mice were bred at the Hospital for Sick Children and group-housed on a 12-h light/dark cycle with food and water *ad libitum*. All experiments took place during the light phase. Primiparous and multiparous dams were used for breeding, and litter birthdate was designated postnatal day (P) 0. Litters ranged in size from 5-12 pups. Occasionally, pups were cross-fostered to different lactating dams on P1-P3 to equalize litter sizes and/or increase experiential diversity of offspring. Cross-fostered rodents receive similar maternal care compared with normally-reared offspring[52]. Preweanling mice (Ages ≤ P20) remained in the breeding cage (identical to standard cages) with the dam for the duration of the experiments. Older mice (Ages ≥ P24) were weaned from the dam on P21 and thereafter group-housed with same-sex littermates in standard mouse housing cages (2-5 mice per cage). To rule out weaning as a potential driver of memory development, in a single experiment (see **Fig. S1I-J**), we weaned mice early on P17 (P20 groups) or did not wean mice (P24 groups). Each experimental condition contained mice derived from 2-8 separate litters, with no more than 2 same-sex littermates used for each experimental condition.

PV-Cre knock-in driver transgenic mice (B6;129P2-*Pvalbtm1(cre)Arbr*/J, Strain# 008069) which express Cre recombinase in PV^+ interneurons, without disrupting endogenous PV expression, were originally generated by Silvia Arber, FMI, and obtained from Jackson Laboratory[53]. Homozygous PV-Cre mouse breeders were maintained on a C57BL/6 background and crossed with 129S6/SvEvTac breeders to generate the hybrid PV-Cre mice used in experiments. Husbandry procedures for this line were identical to those described for WT mice. Acute inhibition of PV^+ interneurons in adult PV-Cre mice expressing hM4Di did not alter the density of perineuronal nets at timepoints relevant to memory encoding and retrieval (see **Fig. S8M-N**). All procedures were approved by the Hospital for Sick Children Animal Care and Use Committee and conducted in accordance with Canadian Council on Animal Care and National Institutes of Health guidelines.

Drugs

DREADD agonist 21 (C21). C21 dihydrochloride (Tocris, cat# 6422) was prepared as a stock solution of 10 mg/ml in dH_2O and stored at -20 °C. Stock solution was later thawed and diluted 1:10 in PBS. Diluted C21 was administered via i.p. injection 1 h before contextual fear training or recall (1.0 mg/kg) to activate or inhibit DREADD-expressing neurons.

Chondroitinase ABC (ChABC). ChABC from *Proteus vulgaris* (Sigma, cat# C3667) was dissolved in 0.1% bovine serum albumin in PBS at a concentration of 50 U/ml. ChABC solution was stored at -80 °C until use.

Penicillinase. Penicillinase from *Bacillus cereus* (Sigma, cat# P0389) was dissolved in 0.1% bovine serum albumin solution (in PBS) at a concentration of 50 U/ml. Penicillinase solution was stored at -80 °C until use.

Recombinant Brain-Derived Neurotrophic Factor (BDNF). Recombinant BDNF (Peprotech, cat# 450-02) was dissolved in PBS at a concentration of 0.36 mg/ml and stored at -80 °C until use.

Viruses

All viruses were made in-house.

Generation of plasmids. To fluorescently label and image extracellular matrix in the noncellular oxidative environment, we subcloned full-length mouse Hapln1 (GeneID: 12950) or ΔHapln1 (mutant lacking the CSPG binding domain) in frame with cysteine-free GFP (cfGFP). The cfGFP plasmid was a gift from Dr. Ikuo Wada[54]. The cDNAs were amplified using the following set of primers: Hapln1 forward primer TAGCGAATTCGCCACCATGAGAAGTCTGCTTCTC and reverse primer TAGCCTCGAGGTTGTATGCTCTGAAGCAATAGACCC; ΔHapln1 forward primer TAGCGAATTCGCCACCATGAGAAGTCTGCTTC and reverse primer TAGCCTCGAGGTTGTATGCTCTGAAGCAATAGACCC; cfGFP forward primer TAAGCACTCGAGGTGAGCAAGGGCGAGGAG and reverse primer TAAGCAGGTACCTTACTTGTACAGCTCGTCCATGC and cloned into a custom-designed AAV vector using appropriate restriction enzymes. The complete plasmid sequences can be found in the supplementary materials. The complete plasmid sequences can be found in the Dryad repository[51] associated with this study.

HSV. We used replication-defective herpes simplex viruses (HSV) to manipulate sparse subsets of CA1 neurons. HSV is naturally neurotrophic and transfects approximately 30% of principal neurons in CA1 following microinjection (see **Fig. S5**). Transgene expression peaks 3-4 days and dissipates after 10-14 d after HSV microinjection[55]. HSV titers were approximately 1.0×10^8 infectious units/ml. The following HSV constructs were used:

HSV-NpACY. We used HSV-NpACY to bidirectionally manipulate the activity of sparse subsets of neurons. HSV-NpACY contains both enhanced channelrhodopsin-2 (ChR2-H134R) fused to enhanced yellow fluorescent protein (eYFP) and halorhodopsin 3.0 (NpHR3.0). These opsins are spectrally compatible, allowing for neuronal excitation by ChR2 with blue light (473 nm) and neuronal silencing by NpHR3.0 with red light (660 nm)[26]. Opsin genes were connected in the viral vector using a 2A self-cleavage linker (p2A) and expression was driven by the endogenous HSV promoter IE4/5.

HSV-NpACY-tdTomato. We used HSV-NpACY-tdTomato instead of HSV-NpACY in select experiments in which a different GFP-expressing viral construct was co-expressed in CA1. HSV-NpACY-tdTomato is identical to HSV-NpACY, with the addition of the tdTomato transgene. In this construct, expression of NpACY was driven by the IE4/5 promoter and expression of tdTomato was driven by a downstream CMV promoter.

HSV-GFP-hM4Di. We used HSV-GFP-hM4Di to inhibit sparse subsets of CA1 neurons. An hM4Di construct, (a gift from Dr. Bryan Roth, University of North Carolina), was subcloned into an HSV-p1006 vector backbone[56]. In the resulting HSV-GFP-hM4Di construct, expression of GFP was driven by the IE4/5 promoter and expression of hM4Di was driven by the downstream CMV promoter.

AAV. We used adeno-associated viruses (AAV) to manipulate neuronal activity or to express our novel Hapln1 constructs. Transgene expression peaks 3-4 weeks after AAV microinjection and is relatively stable in the following weeks. We used a 19-20 d delay allowing roughly equal time for transgene expression following neonatal (P1) or standard surgery protocols. AAVs (DJ

serotype) were generated in HEK293T cells with the AAV-DJ Helper Free Packaging System (Cell Biolabs, Inc., cat# VPK-400-DJ) using the manufacturer-suggested protocol. Viral particles were purified using Virabind AAV Purification Kit (Cell Biolabs, Inc., cat# VPK-140). AAV titers were approximately 1.0 $\times 10^{11}$ infectious units/ml. The following AAV constructs were used:

AAV(DJ)-CaMK2α-iC++-eYFP (AAV-iC++). We used AAV-iC++ to silence CA1 pyramidal neurons in adult mice. pAAV-CaMK2α-iC++-eYFP (a gift from Dr. Karl Deisseroth) was obtained from Stanford Gene Vector and Virus Core. The chloride channel iC++ enables neuronal silencing with blue light (473 nm) and its expression in excitatory principal neurons was driven by the CaMK2α promoter. We did not use AAV-iC++ for neuronal silencing in juvenile mice because we observed increased locomotion in control (GFP-expressing) juvenile mice receiving constant blue light stimulation during fear recall (see **Fig. S3E-F**).

AAV(DJ)-CaMK2α-NpACY (AAV-NpACY). We used AAV-NpACY to silence CA1 pyramidal neurons in juvenile and adult mice. The transgene is identical to that described for HSV-NpACY, enabling neuronal silencing by NpHR3.0 with red light (660 nm). Expression of NpACY in principal neurons was driven by the CaMK2α promoter.

AAV(DJ)-CMV-GFP (AAV-GFP). We used AAV-GFP as a control virus for AAV-iC++ and AAV-NpACY. pAAV-CMV-GFP was a gift from Dr. Connie Cepko (Addgene plasmid # 67634; http://n2t.net/addgene:67634; RRID:Addgene_67634). Expression of GFP was driven by the CMV promoter.

AAV(DJ)-CaMK2α-hM3Dq-mCherry (AAV-hM3Dq). We used AAV-hM3Dq to activate CA1 pyramidal neurons. pAAV-CaMKIIa-hM3D(Gq)-mCherry was a gift from Dr. Bryan Roth (Addgene plasmid # 50476; http://n2t.net/addgene:50476; RRID:Addgene_50476). Expression of hM3Dq-mCherry in principal neurons was driven by the CaMK2α promoter.

AAV(DJ)-hSyn-DIO-hM4Di-mCherry (AAV-DIO-hM4Di). We used AAV-DIO-hM4Di in PV-Cre mice to inhibit CA1 PV^+ interneurons. pAAV-hSyn-DIO-hM4D(Gi)-mCherry was a gift from Dr. Bryan Roth (Addgene plasmid # 44362; http://n2t.net/addgene:44362; RRID:Addgene_44362). Expression of hM4Di-mCherry in Cre^+ interneurons was driven by the neuronal Human synapsin 1 (hSyn) promoter.

AAV(DJ)-hSyn-DIO-mCherry (AAV-DIO-mCherry). We used AAV-DIO-mCherry in PV-Cre mice as a control for AAV-DIO-hM4Di. pAAV-hSyn-DIO-mCherry was a gift from Dr. Bryan Roth (Addgene plasmid # 50459; http://n2t.net/addgene:50459; RRID:Addgene_50459). Expression of mCherry in Cre^+ interneurons was driven by the neuronal hSyn promoter.

AAV(DJ)-hSyn-cfGFP2 (AAV-cfGFP). We used AAV-cfGFP2 as a control for AAV-Hapln1 and AAV-ΔHapln1. pAAV-Syn-cfGFP2 was a gift from Dr. Ikuo Wada (Fukushima Medical University). Cysteine-free GFP (cfGFP) is a modified GFP that reduces protein oligomerization and restriction of free diffusion in the endoplasmic reticulum. Expression of cfGFP2 was driven by the hSyn promoter.

AAV(DJ)-hSyn-Hapln1-cfGFP2 (AAV-Hapln1). We used AAV-Hapln1 to over-express wild-type mouse HAPLN1 protein with cfGFP2. Expression of Hapln1-cfGFP2 was driven by the hSyn promoter.

AAV(DJ)-hSyn-ΔHapln1-cfGFP2 (AAV-ΔHapln1). We used AAV-ΔHapln1 to over-express mutant (dominant-negative) ΔHAPLN1 protein with cfGFP2. ΔHAPLN1 lacks the wild-type N-terminus IgG domain that binds chondroitin sulfate proteoglycans (CSPGs), while maintaining the C-terminus HA1 and HA2 domains that bind to hyaluronic acid (see **Fig. S12A-L**). Expression of Hapln1-cfGFP2 was driven by the hSyn promoter.

Surgery

Surgeries occurred on P1, P16 and/or P17 (P20 groups), P21 (P24 groups), or P40-onwards (P60 or adult groups). Surgical procedures were similar at all ages, except for the neonatal (P1) timepoint. Mice were pre-treated with atropine sulfate (0.1 mg/kg, i.p.), anesthetized with chloral hydrate (400 mg/kg, i.p.) or isoflurane (3% induction, 1-1.5% maintenance), administered meloxicam (4 mg/kg, s.c.) for analgesia, and placed into stereotaxic frames. The scalp was incised and retracted, and holes were drilled above the dorsal CA1. Unless otherwise specified, viruses or drugs were injected bilaterally via a glass micropipette connected via polyethylene tubing to a microsyringe (Hamilton) at a rate of 0.1 μl/min and remained in place for an additional 10 min to ensure virus diffusion. The following coordinates and virus volumes were used for dorsal CA1. For P16-P17: coordinates AP -1.65 mm, ML ±1.35 mm, DV -1.45 mm from bregma; 0.7 μl HSV; or 0.7 μl BDNF (0.25 ng per side[57]) or vehicle (PBS). For P21: coordinates AP -1.7 mm, ML ± 1.4 mm, DV -1.5 mm from bregma; 0.75 μl HSV. For ≥P40: coordinates AP -1.8 mm, ML ±1.5 mm, DV -1.5 mm from bregma; 1.0 μl HSV; 0.85 μl AAV; or 1.0 μl ChABC or Penicillinase. In a subset of experiments we microinjected AAVs, ChABC, or Penicillinase into the CA3, dentate gyrus (DG), prelimbic cortex (PrL), or retrosplenial cortex (RSC) of adult mice using identical procedures. For CA3: coordinates AP -2.2 mm, ML ± 2.7 mm, DV -2.5 mm from bregma; 0.85 μl AAV. For DG: coordinates AP -2.2 mm, ML ±1.65 mm, DV -2.2 mm from bregma; 0.85 μl AAV. For PrL: coordinates AP +1.7 mm, ML ±0.35 mm, DV -1.8 mm from bregma; 0.65 μl AAV at a rate of 0.05 μl/min. For RSC: coordinates AP -1.5 mm, ML ±0.35 mm, DV -1.15 mm from bregma; 1.0 μl ChABC or Penicillinase at a rate of 0.05 μl/min. For western blot experiments, we targeted all subfields of the dorsal hippocampus using coordinates AP -2.0, ML ±2.0, DV -2.2 and -1.5 mm. For each DV site, 1.0 μl of AAV, ChABC, or Penicillinase was injected. Following both microinjections, the scalp was sutured and polysporin was applied to the wound. Mice were administered 0.9% saline (0.5-1.0 ml, s.c.) and placed in a clean cage on a heating pad to recover. Once recovered, the dam was moved to the clean cage (for P16-17 mice), or mice were weaned immediately (for P21 mice).

Neonatal virus injection procedures were adapted from previous studies[21, 58]. P1 mice were anesthetized through hypothermia and mounted to a chilled metal plate using laboratory tape. The scalp was incised and retracted, and the glass micropipette connected to a nanoliter injector (Nanoject III, Drummond Scientific) was used to pierce the skull above dorsal CA1 (approximate coordinates AP -0.5 mm, ML ±0.8 mm from bregma). The pipette was lowered to DV -1.1 from the skull surface, and 0.12-0.15 μl AAV was injected over 1 min and remained in place for an additional 3 min. The scalp was sealed with Vetbond Tissue Adhesive (3M) and covered with polysporin. For some experiments, paws were tattooed using non-toxic black ink for later mouse identification[59]. The entire procedure was performed within 10-12 min. Pups

were placed on a heating pad and continuously monitored until mobile. Pups remained on the heating pad until all surgeries were completed, at which time the litter was returned to the dam.

For optogenetics experiments, optic fibers were implanted above the dorsal CA1 on P17 (P20 groups), P21 (P24 groups), or P53-57 (P60 groups). Implants were constructed in-house by attaching a piece of polished 200 μm diameter optic fiber (0.37 numerical aperture) to a 1.25-mm diameter zirconia ferrule with epoxy resin. Optical fiber implantation was performed immediately following virus injection for HSV experiments or in a second procedure for AAV experiments. Fiber tips were lowered to DV -1.2 mm from bregma above the dorsal CA1 and secured to the skull using screws and black dental cement. Post-surgery procedures and care were the same as described above.

For medial forebrain bundle (MFB) stimulation experiments, unilateral MFB stimulation was conducted as previously described[60]. MFB implants were performed on P16 (P20 groups), P21 (P24 groups), or P53 (P60 groups). Concentric bipolar electrodes were lowered into the right MFB using the following stereotaxic coordinates. For P16 and P21: coordinates AP -1.1 mm, ML 1.0 mm, DV -5.1 mm from bregma. For P53: coordinates AP -1.2 mm, ML 1.0 mm, DV -5.2 mm from bregma. Implants were attached to the skull using screws and black dental cement. Correct placement of the electrodes in the MFB was verified during surgery by brief electrical pulses and by post-hoc identification of electrode tracks in brain slices. Post-surgery procedures and care were the same as described above.

For all experiments involving virus microinjections, only mice showing strong bilateral expression (i.e., expression limited to the target brain region and observable in a minimum of 3 brain sections) were included in the final data set. For experiments in which we infused a combination of HSV and/or AAV constructs, only mice correctly expressing both transgenes in the same region were included in the final data set. Additionally, for optogenetics experiments, only mice with optic fibers placed correctly above the opsin-expressing region of interest were included in the final data set.

Behavior

Fear conditioning. Contextual fear conditioning occurred in test chambers (31 × 24 × 21 cm) with shock-grid floors (Med Associates). Unless otherwise stated, mice were trained in a single 5-min session with three foot shocks. During training, mice were placed in the chambers for 2 min, after which three foot shocks (0.5 mA, 2 s duration, 1 min apart) were delivered. Mice were removed from the chambers 1 min after the last shock. The next day, mice were placed in one of four different test chamber configurations for 5 min or 6 min (for optogenetics experiments). In most experiments, testing occurred in the training chamber (Context A) or a similar but novel chamber (Context B). Context B was approximately the same size as Context A, with white plastic floor and triangular white plastic walls. Two novel, dissimilar contexts were used for specific experiments. Context C was a rectangular chamber (15 × 45 × 25 cm) with an open top, made of white plexiglass, and was located in a separate room. Context D was a test chamber with white plastic floor and a semi-circular white plastic wall, with speakers for auditory tone presentation. Context D chambers were located in another separate testing room and placed inside of sound-attenuating boxes. Mouse behavior was recorded with overhead cameras and FreezeFrame v.3.32 software (Actimetrics). For contextual fear memory tests, the amount of time mice spent freezing was scored during the entire test session automatically using FreezeFrame

software or manually (for optogenetics experiments). Freezing was defined as the cessation of movement, except for breathing[61]. Specific details for experiments deviating from the standard protocol are described below.

To test whether juvenile mice's potentially different learning rate or training intensity accounts for their memory imprecision, we modified the training protocol for P20 and P60 mice to account for differences in freezing after training (see **Fig. S1A-G**). After 2 min in the chamber, P20 mice received one foot shock (0.5 mA, 2 s duration) or P60 mice received 5 foot shocks (0.5 mA, 2 s duration, 1 min apart), and were removed after 1 min. Testing occurred as described above.

To test whether juvenile mice's lack of familiarity with the test chambers accounts for their memory imprecision, we pre-exposed mice to chambers before fear conditioning (see **Fig. S1K-O**). Context pre-exposure is an experiential manipulation known to increase memory precision in adult rats and mice[62, 63]. Mice were pre-exposed to Contexts A and B (order counterbalanced) on P19 (P20 groups) or P23 (P24 groups) for 5 min each with 5-6 h between exposures (Pre groups). Control mice were not pre-exposed to either context before training (No-Pre groups). Training and testing began the following day as described above.

To test whether juvenile mice formed imprecise short-term memories, we reduced the time interval between training and testing (see **Fig. S1R-S**). P20 and P60 mice were tested 1 h after training.
To test whether memory imprecision in juvenile mice extended to all novel environments, we tested mice in a novel, dissimilar chamber (see **Fig. S1T-U**). Following training, P20, P24, and P60 mice were tested in Context C.

To test whether the effects of CA1 PNN disruption were specific to contextual and spatial memories, we trained adult mice expressing ΔHapln1 or cfGFP in auditory fear conditioning (see **Fig. S15C-D**) as previously described[26]. During training, mice were placed in the conditioning chamber for 2 min before the presentation of a 30 s auditory tone (2.8 kHz tone, 85 dB; Tone A) that co-terminated with a foot shock (0.5 mA, 2 s duration). Mice remained in the chamber for an additional 30 s after the shock. For the test, mice were placed into Context D, and after 2 min, presented with Tone A or a novel auditory stimulus (7.5 kHz pips, 5 ms rise, 75 dB; Tone B) for 1 min. Freezing behavior to Tone A and Tone B were scored automatically.

Optogenetic stimulation (contextual fear conditioning). Mice used in the optogenetics experiments were habituated to the optic patch cables for 5 min on the day before training. For optogenetic-mediated allocation experiments, the allocation procedure was performed immediately before training in the contextual fear conditioning task. Mice were attached to the optic patch cables and placed into a clean cage. $NpACY^+$ neurons in these mice were briefly excited with blue light (473 nm, 1 mW, 4 Hz, 15-ms pulses) for 30 s. This stimulation frequency was chosen based on previous reports[18, 64]. Non-allocated, Control mice were attached to the optic patch cables but did not receive light stimulation. Mice were detached from the optic patch cables and trained immediately as described above. We verified that optogenetic-mediated allocation before training results in increased localization of training-induced c-Fos in $NpACY^+$ neurons (see **Fig. S6B-E**). For optogenetic stimulation during testing, mice were attached to the patch cables and placed in the test chamber (Context A or Context B) for a 6 min period. For the first 3 min of the test session, no light was applied. For the latter 3 min of the test, continuous

blue (473 nm, 7-10 mW) or red (660 nm, 7-10 mW) light stimulation was delivered to silence the iC++$^{+}$ or NpACY^{+} neurons in CA1. Freezing behavior during these memory tests was scored manually by an experimenter blinded to the experimental conditions (except Age, which could not be blinded).

Exploratory habituation. To determine whether juvenile mice could perceptually discriminate similar spatial environments, we performed a non-associative exploratory habituation task (see **Fig. S1P-Q**). P20 and P60 mice were placed in a rectangular shuttle box (15 × 45 × 25 cm) with white and black-and-white striped compartments and allowed to freely explore for 5 min (Exposure 1). 24 h later, mice were placed into the same shuttle box (Context A) or a different shuttle box with light and dark compartments (Context B) for 5 min (Exposure 2). Mouse behavior was recorded using overhead cameras and the distance traveled during the 5-min sessions was scored automatically using Limelight software (Actimetrics). Because distance traveled was overall lower for P20 mice compared to P60 mice (data not shown), we quantified exploratory habituation to the environments by computing a Habituation Index (Exposure 2 Distance / Exposure 1 Distance) where a score of 1.0 indicates no change in exploration and scores less than or more than 1.0 indicate exploratory habituation or sensitization, respectively.

Inhibitory Avoidance (IA). Inhibitory avoidance was performed as previously described[55]. The IA apparatus was a rectangular shuttle box (25.5 × 16.5 × 17.7 cm) designed similarly to the shuttle boxes used for exploratory habituation experiments. The IA shuttle box consisted of two compartments (safe and shock compartments) separated by a sliding door. The safe compartment was white and illuminated and the shock compartment was black and covered to prevent light entry. On the training day, mice were placed in the safe compartment with their heads facing away from the closed door, and after 10 s, the door was opened. The sliding door was shut 1 s after mice entered the shock compartment, and a single 1 mA (2 s duration) foot shock was delivered. Mice remained in the shock compartment for 10 s following the foot shock and then were returned to their home cage. The next day, mice were tested using the training IA shuttle box (Context A) or a modified shuttle box (Context B). The walls of the Context B shuttle box were curved and Context B similarly contained light- and dark-colored compartments separated by a sliding door. Mice were placed in one of the test apparatuses in the illuminated compartment, and after 10 s the sliding door was opened. The latency (in s) of the mice to enter the dark compartment from the time of door opening was examined for the training and testing sessions.

Spatial Foraging Task. The spatial foraging task was designed similarly to the hippocampus-dependent Morris water maze task[65]. In contrast to the Morris water maze task, performance in the spatial foraging task is appetitively-motivated and allows for easier manipulation of the testing environments. Mice were handled and habituated to the stimulation patch cord for 15 min/day for 3 (P20 and P24 groups) or 7 (P60 groups) days before training. Training occurred in a white, square arena (100 × 100 × 40 cm for P60 groups or 42 × 42 × 30 cm for P20 and P24 groups) located in a dimly lit room (see **Fig. S2A**). The arena was surrounded by white curtains painted with four distinct visual cues, located 1 m away from the perimeter of the arena. The arena was divided into quadrants, and a circular reward zone (11 cm in diameter for P60 groups and 6 cm in diameter for P20 and P24 groups) was located in the center of one of the four quadrants during training. On the training day, mice received 20 training trials that were 3 min in duration each. Electrical stimulation of the MFB was designed to approximate high-frequency brain stimulation (139 Hz, 90-μs pulses). During the first trial, mice

were connected to the stimulating patch cord, placed into the reward zone, and MFB stimulation was delivered. This was done to expose mice to MFB stimulation within the arena's reward zone. On subsequent trials, mice were placed in one of four pseudo-randomly chosen starting locations and allowed to explore freely. MFB stimulation was delivered upon entry into the reward zone and was terminated once mice left the reward zone. If mice failed to find the reward zone within 60 s from the trial start, they were gently guided by the experimenter to the location. Twenty-four-h later, a 60-s probe trial was conducted in the training arena (Context A) or a novel circular arena (Context B) placed in the same position as the training arena (i.e., with the same distal visual cues). Mice were placed in the quadrant furthest from the reward zone during training and allowed to freely explore the testing arena, with no delivery of MFB stimulation. In one experiment, we removed the visual cues from the curtain surrounding the testing arena to demonstrate that performance in the spatial foraging task (like the Morris water maze) is dependent on the use of distal spatial cues (see **Fig. S2F-H**).

Behavioral data from the spatial foraging task were acquired and analyzed using custom software. For training, latency to reach the reward zone (in seconds, maximum of 60 s) was recorded. For the probe trial, we quantified spatial memory precision by measuring time spent in the target quadrant, defined as the amount of time mice spent searching in the arena quadrant that previously held the reward zone in the training Context A or the equivalent quadrant in the novel Context B (chance performance = 25%).

Open field and Elevated-plus maze. To control for the possibility that PNN manipulations alter locomotion or anxiety-like behaviors, we examined mouse behavior in an open field and on an elevated plus maze. The open field was a square arena (45 × 45 × 20 cm) located in a dimly lit room. Mice were placed in the center of the arena and allowed to explore for 10 min. The locomotion of the mice was tracked using an overhead camera. The total distance traveled (normalized to the mean distance of the control group) and amount of time spent in the center of the arena were obtained with Limelight software (Actimetrics). The next day, mice were placed in the center of the elevated plus maze and behavior was monitored for 5 min. The total distance traveled (normalized to the mean distance of the control group) and amount of time spent in the open arms of the maze were obtained using an overhead camera and Ethovision software (Noldus). For both the open field and elevated-plus maze, a reduction in distance traveled or time spent in the center or open-arm regions are considered to reflect an anxiety-like phenotype.

Histology

Perfusion and tissue preparation. At the appropriate age, following the appropriate delay (for viral or drug manipulations), or following behavior experiments, mice were transcardially perfused with chilled 1× PBS followed by 4% paraformaldehyde (PFA), fixed in PFA overnight at 4 °C, and transferred to 30% sucrose solution for at least 48 h. PBS and PFA volumes were adjusted for different mouse ages. When appropriate, perfusions were timed to occur 60 min, 90 min, or 24 h after contextual fear conditioning training or testing. Brains were sectioned coronally using a cryostat (Leica CM1850), and a ¼ sampling fraction was used to obtain 4 sets of 50-μm sections. Sections for immunohistochemistry were stored at 4 °C in PBS containing 0.1% NaN_3 until staining.

Immunohistochemistry. Immunofluorescence staining was conducted as previously described[26]. For experiments involving quantification of the number of cells positive for immunofluorescence

or immunofluorescence signal intensity, all staining was performed at once using the same antibody solutions. Free-floating sections were blocked with PBS containing 4% normal goat serum and 0.5% Triton-X for 1 h at room temperature. Afterwards, sections were incubated with primary antibodies in fresh blocking solution: rabbit anti-c-Fos (1:1000, Synaptic Systems, cat# 226003), rabbit anti-Arc (1:1000, Synaptic Systems, cat# 156003), chicken anti-GFP (1:1000, Aves, cat# GFP-1010), mouse anti-RFP (1:1000, Rockland Immunochemicals, cat# 200-301-379), rabbit anti-RFP (1:1000, Rockland Immunochemicals, cat# 600-401-379), mouse anti-PV (1:1000, Sigma, cat# 1572), rabbit anti-PV (1:1000, Swant, cat# PV27), guinea-pig anti-PV (1:1000, Swant, cat# GP72), mouse anti-Syt2 (1:1000, ZIRC, cat# znp-1), mouse anti-CaMK2α (1:200, Sigma, cat #C265), biotinylated WFA (1:1000, Sigma, cat# L1516), rabbit anti-ACAN (1:1000, Sigma, cat# AB1031), rabbit anti-BCAN (1:1000, a gift from Dr. Renato Frischknecht), and mouse anti-HAPLN1 (1:100, R&D Systems, cat# MAB2608) for 24 h or 72 h (for c-Fos experiments) at 4 °C. Sections were washed three times for 15 min each with PBS containing 0.1% Tween-20 (PBST), then incubated with PBST containing secondary antibodies: goat anti-chicken Alexa Fluor 488 (1:500, Invitrogen, cat# A-11039, goat anti-mouse Alexa Fluor 488 (1:500, Invitrogen, cat# A-11001), goat anti-mouse Alexa Fluor 568 (1:500, Invitrogen, cat# A-11004), goat anti-mouse Alexa Fluor 647 (1:500, Invitrogen, cat# A-21235), goat anti-rabbit Alexa Fluor 488 (1:500, Invitrogen, cat# A-11008), goat anti-rabbit Alexa Fluor 568 (1:500, Invitrogen, cat# A-11011), goat anti-mouse Alexa Fluor 647 (1:500, Invitrogen, cat# A-21244), goat anti-mouse Alexa Fluor 488 (1:500, Invitrogen, cat# A-11001), goat anti-guinea pig Alexa Fluor 647 (1:500, Invitrogen, cat# A-21450), streptavidin Alexa Fluor 405 (1:500, Invitrogen, cat# S-32351), streptavidin Alexa Fluor 488 (1:500, Invitrogen, cat# S-11223), streptavidin Alexa Fluor 568 (1:500, Invitrogen, cat# S-11226), streptavidin Alexa Fluor 647 (1:500, Invitrogen, cat# S-32357) for 2 h at room temperature. Sections were washed with PBS, counterstained with DAPI, mounted on gel-coated slides, and coverslipped with Permafluor mounting medium (ThermoFisher Scientific, cat# TA-030-FM).

Imaging. Images were obtained using a confocal laser scanning microscope (LSM 710; Zeiss). For visualization of virus expression, images were acquired with a 20× objective. For image quantification, z-stacks were acquired using a 40× objective (N.A. = 1.3; 15-40 slices with a 1 μm step size), except for one set of experiments in which images acquired with the 20× objective were used for quantification (see **Fig. S9**). For all experiments involving quantification of the number of cells positive for immunofluorescence or immunofluorescence signal intensity, all images were acquired using identical imaging parameters (laser power, photomultiplier gain, pinhole, and detection filter settings) in a minimal number of imaging sessions (when possible, in one session). For each experiment, imaging parameters were set using a sample section from a control mouse. In experiments where the dependent variable was mouse age, P60 was considered the 'control' group.

Quantification. For cell counting experiments in the CA1, CA3, or DG, every fourth section was assessed for the marker(s) of interest. For each mouse, cells were counted manually in Fiji (National Institutes of Health) using 5 images acquired from 3-5 sections and averaged. To estimate the number of $DAPI^+$ cells in the CA1 pyramidal layer, $DAPI^+$ cells were counted in a small volume (approximately 12-20 $\times 10^3$ μm^3) to obtain the $DAPI^+$ density (mm^{-3}) for each Age group (see **Fig. S4E**). For all experiments, the volume of the pyramidal layer within each image was measured and multiplied by the $DAPI^+$ density value for the appropriate age group to obtain the estimated $DAPI^+$ cell number. Quantification of c-Fos^+ cells was limited to the pyramidal

layer, whereas all other markers were quantified in all visible layers. The proportion of pyramidal layer cells expressing c-Fos after contextual fear conditioning training, test, or in the home cage are reported as $P(\text{c-Fos}^+|\text{DAPI}^+)$. The proportion of NpACY^+ cells expressing c-Fos after contextual fear conditioning training in Allocation and No Allocation groups are reported as $P(\text{c-Fos}^+|\text{NpACY}^+)$. The number of PV^+ interneurons and WFA^+, BCAN^+, or HAPLN1^+ PNNs are reported per volume (mm^{-3}). Colocalization of the same PNN markers with PV^+ interneurons are reported as $P(\text{marker}^+|\text{PV}^+)$.

To examine how PV^+ interneuron processes mature with age or are affected by PNN manipulations, we quantified the density of PV^+ neurites or Syt2^+ synaptic puncta labeling within the CA1 pyramidal layer[66, 67]. PV^+ or Syt2^+ immunofluorescence was binarized in Fiji using a gray value threshold that was manually determined using an image from a mouse in the control or P60 group. The same threshold was applied to all images belonging to the same experiment. We measured the percentage of pyramidal layer area covered by PV^+ or Syt2^+ labeling in 15 ROIs per mouse (3 per image, approximately 400 μm^2 each) and averaged the data to obtain a single data point. For each image (z-stack), ROIs were drawn in z-slice with the greatest immunofluorescence and excluded any areas containing PV^+ somas.

To examine the structural plasticity of PV^+ neurites after contextual fear conditioning training, we quantified the density of PV^+ neurite in the perisomatic region of CA1 pyramidal layer cells, similar to previous studies[26, 68, 69]. PV^+ immunofluorescence was binarized in Fiji as described above. To quantify the extent of perisomatic PV innervation surrounding c-Fos^+ and an equal number of c-Fos^- cells in the pyramidal layer (50-150 cells per mouse), the DAPI^+ nucleus of cells were outlined and the percentage of area covered by PV^+ labeling within a 3-μm band was measured. c-Fos^+ and c-Fos^- cells were approximately matched by selecting c-Fos^- cells in close proximity to (within 2 nuclei away) and adjacent to (and not above or below) a corresponding c-Fos^+ cell. Perisomatic PV^+ labeling surrounding c-Fos^+ and c-Fos^- cells were averaged independently for each mouse and used to compute the Perisomatic PV^+ Selectivity (mean c-Fos^- labeling / mean c-Fos^+ labeling). As a control experiment, we performed the same analysis using P20 and P24 mice that were not trained, except using 20-80 cells per mouse, as the number of c-Fos^+ cells in P24 mice taken from the home cage was very low.

In vitro **binding experiments**

Preparation of HAPLN1-, ΔHAPLN1-, and cfGFP-enriched media. One day prior to transfection, HEK293 cells were cultured in Iscove's Modified Dulbecco's Medium (IMDM) supplemented with 10% fetal bovine serum (FBS) and 1% L-Glutamine at a density of 3.0×10^6 cells per 10 cm Petri dish. Cells were transfected using polyethyleneimine (PEI) with 10 µg of the corresponding plasmid DNA per 10 cm Petri dish. After 7 h of transfection, the culture medium was replaced with serum-free IMDM supplemented with 1% L-Glutamine.

Culture medium was collected 48 h after transfection and protease inhibitor cocktail (Roche Diagnostics GmbH, Mannheim, Germany, cat# 11836153001) was added according to the manufacturer's instructions. The collected medium was then concentrated using Amicon® 10k centrifugal filters (Merck Millipore Ltd., County Cork, Ireland, cat# ufc801024). The buffer was then exchanged with PBS containing a protease inhibitor cocktail using the same columns. Finally, the resulting protein solutions were aliquoted and stored at -20 °C.

Western blot. Samples of HAPLN1-, ΔHAPLN1-, and cfGFP-enriched media were diluted and supplemented with SDS sample buffer (50 mM Tris-HCl pH 6.8, 2% SDS, 1% β-mercaptoethanol, 5% glycerol, bromophenol blue) and then boiled for 5 min at 95 °C. The resulting samples were then loaded onto a 12% protein gel. The gels were run in Tris-glycine buffer (25 mM Tris, 192 mM glycine, 0.1% SDS, pH 8.3) at 100 V. The separated proteins were transferred onto a nitrocellulose membrane (Bio-Rad, cat# 1704270) using a Trans-Blot Turbo Transfer System (Bio-Rad, cat# 1704150). After transfer, the membrane was blocked with 5% skim milk (SERVA Electrophoresis GmbH, Heidelberg, Germany, cat# 42590.01) in 0.1% Tween-20 in TBS (TBST) for 1 h at room temperature. The membrane was then incubated overnight at 4 °C with gentle shaking in primary antibody to GFP (1:1000, BioRAD, cat# 4745-1051) in 1% skim milk/TBST solution.

The next day, the membrane was washed three times with TBST and then incubated with the horseradish peroxidase-conjugated donkey anti-sheep secondary antibody (1:10000, Jackson ImmunoResearch, cat# 713-035-003) in 1% skim milk/TBST for 3 h at room temperature with gentle shaking. After three additional washes with TBST, the membrane was developed using SuperSignal West Pico PLUS Chemiluminescent Substrate (ThermoFisher Scientific, cat #34580) and imaged using the Azure Biosystems c300 imaging system.

Preparation of mouse brain lysate. Three-week-old C57BL/6 mice were rapidly decapitated, and their brains were immediately washed with ice-cold PBS. Subsequently, the brains were homogenized in lysis buffer containing 50 mM Tris-HCl pH 7.5, 150 mM NaCl, 1% Triton X-100, and 1× protease inhibitor cocktail. The homogenate was centrifuged at 14,000 rpm for 30 min at 4 °C to collect the resulting supernatant. The supernatant was then concentrated using Amicon® 100K filter columns.

Binding analysis of lectican-HAPLN1 complexes and hyaluronic acid. 96-well plates (FluoroNunc MaxiSorp, ThermoFisher Scientific, cat# 475515) were rinsed with PBS four times using 400 µl in each well. 100 µl of hyaluronic acid solution (1 mg/ml in PBS, Sigma, cat# H5388-100MG) was added to each well and plates were covered with a film (ELISA Plate Covers, Immunochemistry Technologies, cat# 6287). Plates were incubated overnight at 4 °C with moderate shaking (250 rpm, Ika MS3 digital, cat# 0003319000). The following day, wells were rinsed with PBS four times using 400 µl per well. The 96-well plates were then blocked with a 2% BSA in PBS solution and incubated for 2 h at room temperature.

To prepare HAPLN1 and brain lysate mixtures, required amounts of HAPLN1-, ΔHAPLN1-, or cfGFP-enriched media and brain lysate were mixed in 1.5 ml tubes. The mixtures were diluted in dilution buffer (DB; TBST containing 1% BSA and protease inhibitor cocktail) and incubated for 2 h at 37 °C with moderate shaking (500 rpm, Mixing block mb-102, Biozym).

After blocking, the plates were rinsed with wash buffer (TBST with 0.1% BSA) four times using 400 µl per well. 100 µl of preincubated HAPLN1/brain lysate mixture was added to each well and plates were covered with a film. The plates were incubated for 2 h at 37 °C with moderate shaking (250 rpm, Ika MS3 digital, cat# 0003319000). After incubation, the plates were rinsed with wash buffer four times using 400 µl in each well.

Primary antibodies including rabbit anti-ACAN (1:500, Milipore, cat# AB1031), guinea pig anti-BCAN (1:1000, a kind gift of Drs. Constanze Seidenbecher[70] and Renato Frischknecht),

sheep anti-NCAN (1:1000, R&D Systems, cat# AF5800), and sheep anti-GFP (1:1000, BioRad, cat# 4745-1051) were diluted in DB and 100 µl of each solution was added to the corresponding wells. The plates were covered with a film and incubated for 2 h at 37 °C with moderate shaking (250 rpm). After incubation, the plates were rinsed with wash buffer four times using 400 µl in each well.

100 µl of secondary antibodies were added to each well: Peroxidase AffiniPure donkey anti-sheep (1:10000, Jackson ImmunoResearch, cat# 713-035-003), Peroxidase AffiniPure goat anti-rabbit (1:5000, Jackson ImmunoResearch, cat# 111-035-144); Peroxidase AffiniPure goat anti-guinea pig (1:10000, Jackson ImmunoResearch, cat# 106-035-003). The plates were covered with a film and incubated for 2 h at 37 °C with moderate shaking (250 rpm). After incubation, the plates were rinsed with wash buffer 4 times, using 400 µl per well.

Finally, the plates were developed using SuperSignal West Pico PLUS Chemiluminescent Substrate (ThermoFisher Scientific, cat #34580) with 100 µl per well, and chemiluminescence intensity was measured using Fluorostar Optima (BMG Labtech, Ortenberg, Germany). All the results shown are based on the measurements of at least two independent plates.

Binding analysis of HAPLN1 and hyaluronic acid. Binding of HAPLN1 isoforms to hyaluronic acid was performed as described above with a few modifications: HAPLN1 isoforms were not preincubation with brain lysate, HAPLN1 isoforms were incubated with preabsorbed hyaluronic acid for 1 h at room temperature, and antibodies were incubated at room temperature.

Western Blot

Three weeks following AAV microinjections or 24 h following ChABC or Penicillinase microinjections, mice were rapidly decapitated, and their hippocampi were dissected and flash frozen in liquid nitrogen. Dorsal hippocampi were sonicated in homogenization buffer (50 mM Tris-HCl pH 7.5, 0.25 M sucrose, 25 mM KCl, 5 mM MgCl2) supplemented with protease inhibitor cocktail (BioShop, cat# PIC002). Homogenized samples were centrifuged at 14,000 rpm for 15 min at 4 °C and the protein concentration of the supernatant was determined by Pierce BCA Protein Assay (ThermoFisher Scientific, cat# 23227). Samples were diluted and supplemented with SDS sample buffer (50 mM Tris-HCl pH 6.8, 2% SDS, 1% β-mercaptoethanol, 5% glycerol, bromophenol blue). Protein samples (25 µg) were separated by electrophoresis on 4-15% mini-PROTEAN TGX precast gels (Bio-Rad, cat# 456-1083) and transferred to PVDF membranes (Bio-Rad, cat# 162-0177). Membranes were blocked with 5% skim milk in Tris-buffered saline with 0.1% Tween-20 (TBS-T) for 1 h at room temperature. Membranes were incubated in primary antibodies diluted in 5% skim milk in TBST: mouse anti-BCAN (1:1000, BioLegend, cat# 820101), sheep anti-NCAN (1:1000, R&D Systems, cat# AF5800), goat anti-HAPLN1 (1:1000, R&D Systems, cat# AF2608), rabbit anti- β-actin (1:1000, Cell Signaling Technology, cat# 4967) overnight at 4 °C or for 1 h at room temperature. Membranes were incubated with horseradish peroxidase (HRP)-conjugated secondary antibodies diluted in 5% skim milk in TBST: horse anti-mouse IgG (1:20,000, Cell Signaling Technology, cat# 7076), donkey anti-sheep IgG (1:20,000, Invitrogen, cat# A16041), donkey anti-goat IgG (1:20,000, Invitrogen, cat# A15999), and goat anti-rabbit IgG (1:20,000, Sigma, cat# A0545) for 1 h at room temperature. Protein bands were visualized with Amersham ECL Prime Western Blotting Detection Reagent (Cytiva, cat# RPN2236) and chemiluminescence was imaged with a ChemiDoc XRS+ System (Bio-Rad). Band intensities were quantified using Image Lab 6.1 software (Bio-Rad). The intensities of the proteins of interest were normalized to the intensity of

the loading control, actin, and normalized to the mean intensity of the control condition in each experiment (AAV-cfGFP or Penicillinase).

Statistical Analyses

No statistical tests were used to predetermine sample sizes, but our sample sizes were similar to those reported in previous publications[26, 27, 55]. Mice were pseudo-randomly assigned to all groups, except when the dependent variable was age, to achieve roughly equivalent group sizes. During data collection and quantification, experiments were blinded to group assignment, except for age and testing context during data collection and testing context during quantification. The key findings (maturational changes in memory precision, engram sparsity, PV^+ interneurons, and PNNs) were replicated multiple times throughout the study, and different methods were used to provide converging evidence for the role of hippocampal PNN maturation in the development of memory precision.

Data were analyzed using one-way or factorial analysis of variance (ANOVA) with repeated measures when appropriate. When appropriate, ANOVAs were followed by Newman-Keuls post-hoc comparisons. In one instance, we used planned *t*-tests based on strong *a priori* predictions (see **Fig. 6L**). In some experiments, we pooled control mice into a single control group (see **Fig. S8M-N** and **S13J-K**). Sub-group means were not statistically different from one another (data not shown). For the analyses of potential sex differences in memory precision or PNN development (see **Fig. S1H**, **S10A**), data were pooled from different experiments (**Fig. 1C, S1M** [No Pre Group], **S1O** [No Pre Group] and **Fig. 4C, S10C**) to attain sufficiently large sample sizes, and re-analyzed. Subjects pooled into the same groups for the analysis of potential sex differences were treated identically across the different experiments.

For the saturation binding experiment (see **Fig. S12C**), data were plotted as Dilution of the corresponding HAPLN1 isoform vs. GFP intensity (A.U.). Data for HAPLN1 and ΔHAPLN1 were fitted using one-site binding models:

$$GFP\ intensity = \frac{B_{max} \times Dilution}{K_d + Dilution}$$

where B_{max} is the maximum level of specific binding (in A.U. of chemiluminescence) and K_d is the equilibrium dissociation constant. B_{max} and K_d parameters are reported with 95% confidence intervals (CI). Model comparisons based on Akaike Information Criterion (AIC) were used to determine whether the fitted binding curves, B_{max}, and K_d for HAPLN1 and ΔHAPLN1 differed.

Statistical significance was set at $P < 0.05$, and Bonferroni correction was applied when appropriate. Statistical analyses were performed using Statistica software (Dell Inc. 2016, version 13) and Graphpad Prism (version 8.0.1).

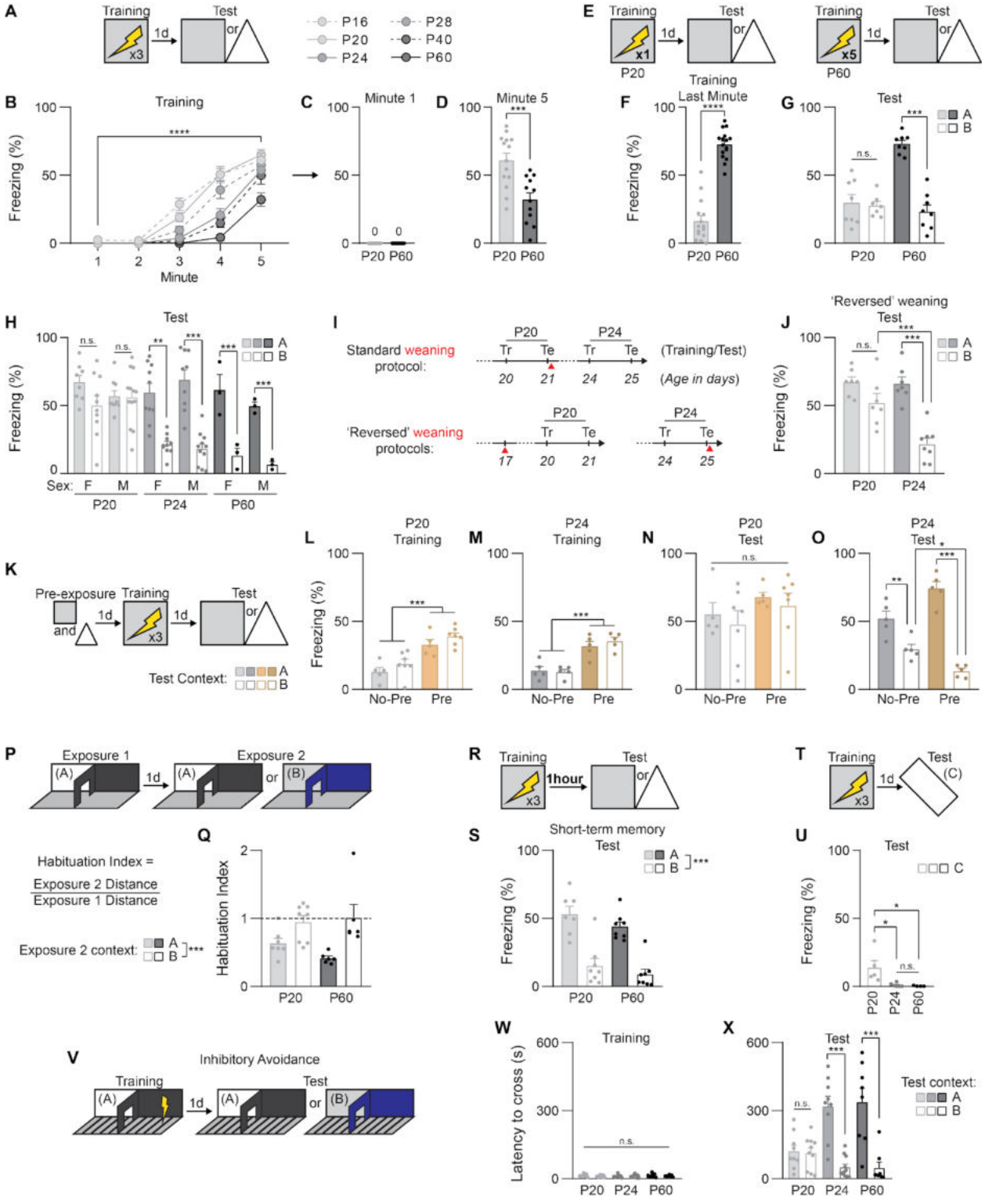

Figure S1. Behavioral characterization of contextual fear memory precision development (Related to Figure 1). (A to D) Training data related to Figure 1C. Schematic of the contextual fear conditioning protocol (A). All age groups showed increased freezing across the 5-min training session (B, ANOVA, Age × Minute interaction: $F_{20,304} = 6.81$, $P < 10^{-6}$). P20 and P60 mice exhibited no freezing behavior during the first minute of the training session (C), but P20

mice froze more than P60 mice during the last minute of the training session (D, unpaired *t*-test: $t_{24} = 4.01$, $P < 0.001$). **(E to G)** The contextual fear conditioning protocols were modified to account for potential age-related differences in learning (E). Decreasing and increasing the number of shocks delivered to P20 and P60 mice, respectively, resulted in greater freezing in P60 mice during the last minute of the training session (F, unpaired *t*-test: $t_{29} = 12.09$, $P < 0.0001$), but did not alter memory precision at either age (G, ANOVA, Age × Test Context interaction: $F_{1,27} = 29.46$, $P < 0.0001$). **(H)** The development of memory precision by P24 was not sex-dependent (ANOVA, Age × Test Context interaction: $F_{2,80} = 12.45$, $P < 0.0001$). **(I to J)** Weaning status in P20 and P24 groups (I), did not alter the development of memory precision (J, ANOVA, Age × Test Context interaction: $F_{1,25} = 8.48$, $P < 0.01$). **(K to O)** Pre-exposure to the testing contexts (K) improved encoding of fear memories in P20 (L, ANOVA, main effect of Pre-exposure: $F_{1,20} = 37.70$, $P < 10^{-5}$) and P24 (M, ANOVA, main effect of Pre-exposure: $F_{1,16} = 48.90$, $P < 10^{-5}$) mice. Context pre-exposure did not ameliorate memory precision in P20 mice (N, ANOVA, $P > 0.05$) but improved memory precision in P24 mice (O, ANOVA, Pre-exposure × Test Context interaction: $F_{1,16} = 19.90$, $P < 0.001$). **(P to Q)** P20 and P60 mice successively exposed to the same or different similar environments (P) showed equal levels of exploratory habituation and dishabituation (Q, ANOVA, main effect of Exposure 2 Context: $F_{1,23} = 16.64$, $P < 0.001$). **(R to S)** Shortening the retention interval between training and testing to 1 hour (R) revealed precise short-term contextual fear memories in P20 mice (S, ANOVA, main effect of Test Context: $F_{1,27} = 62.13$, $P < 10^{-6}$). **(T to U)** P20 mice tested in an environment dissimilar to the training context (T) showed little freezing behavior but froze more than P24 and P60 mice (U, ANOVA, main effect of Age: $F_{2,12} = 6.17$, $P < 0.05$). **(V to X)** In an inhibitory avoidance task (V), all mice had similar crossing latencies during training (W, ANOVA, $P > 0.05$). During testing, P20 mice had imprecise inhibitory avoidance memories compared to P24 and P60 mice, which showed lower crossing latencies in the novel shuttle box (X, ANOVA, Age × Test Context interaction: $F_{2, 49} = 10.78$, $P < 0.001$). Data points are individual mice with mean ± s.e.m. * $P < 0.05$; ** $P < 0.01$; *** $P < 0.001$, **** $P < 0.0001$.

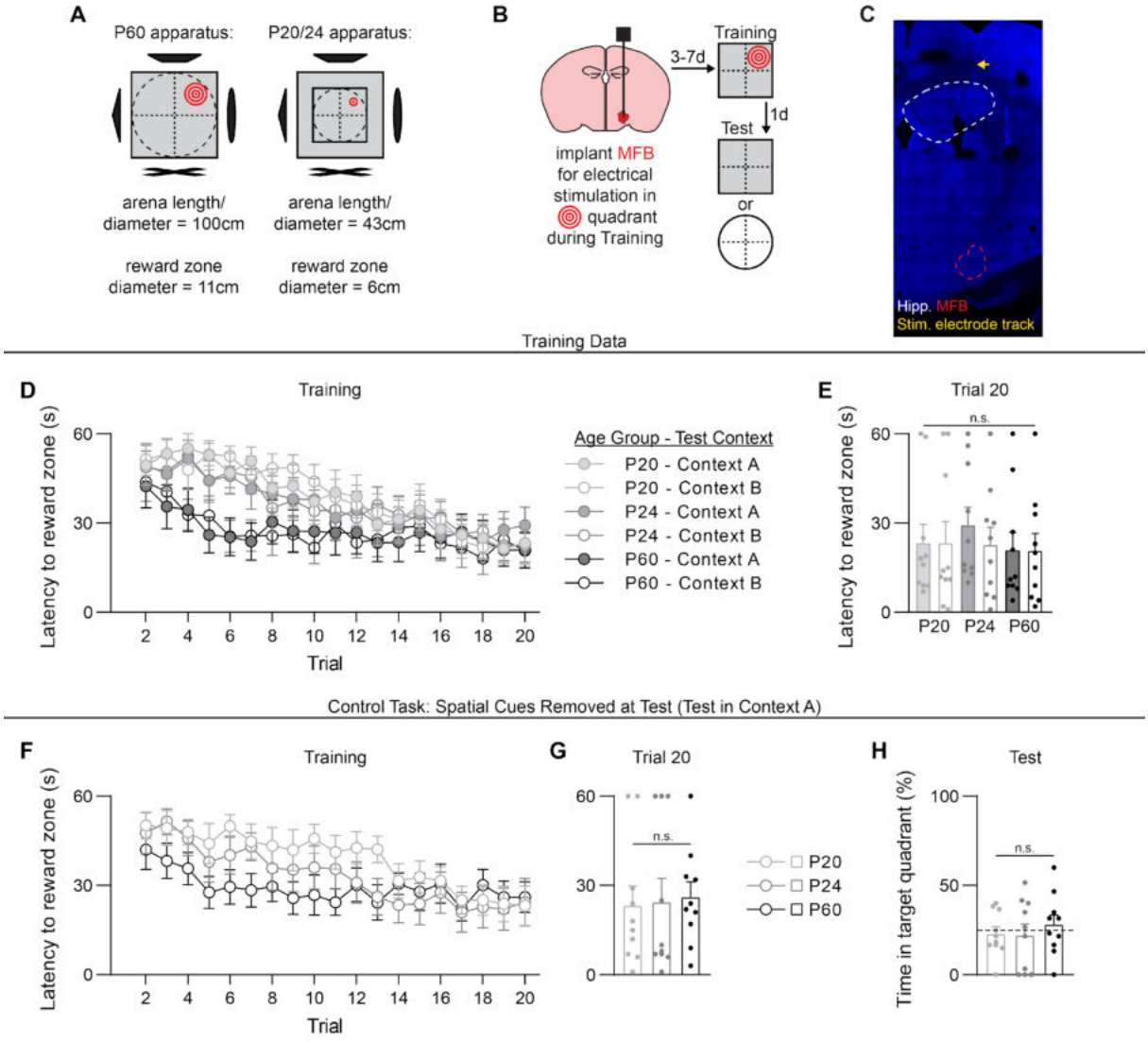

Figure S2. Spatial foraging task training data (Related to Figure 1). (A) Schematic of testing apparatuses used for the spatial foraging. **(B)** Mice were implanted with stimulating electrodes targeting the medial forebrain bundle (MFB) days before training and testing. **(C)** Electrode tracks above the MFB in the brain of a P60 mouse. **(D to E)** Latencies to locate the reward zone decreased across training trials in all groups (D) and did not differ across groups by the last training trial (E, ANOVA, $P > 0.05$). **(F to H)** Different groups of mice were trained in the spatial foraging task as before. Latencies to locate the reward zone decreased across trials (F) and did not differ across groups by the last training trial (G, ANOVA, $P > 0.05$). When tested in Context A with the distal spatial cues removed, all groups performed at chance levels (H, ANOVA, $P > 0.05$). Data points are individual mice with mean ± s.e.m.

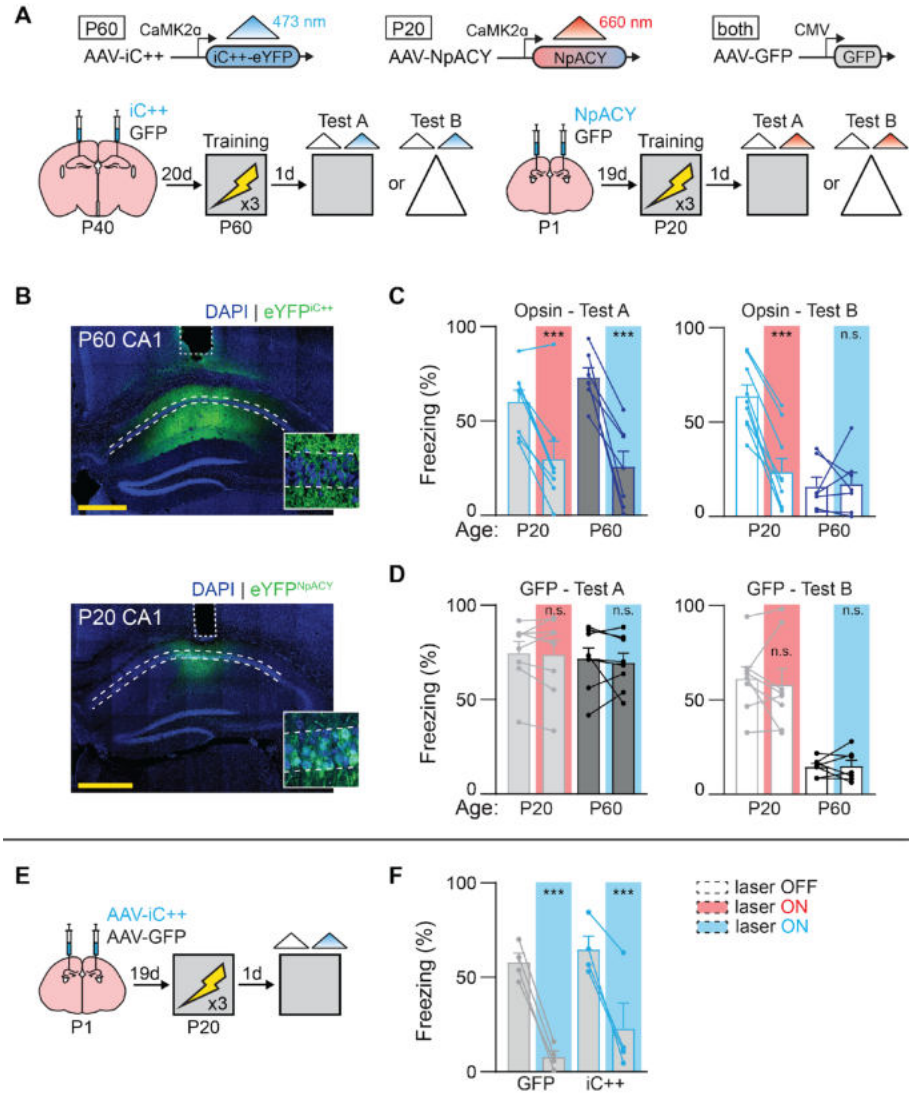

Figure S3. The dorsal CA1 is required for contextual fear memory recall in adult and juvenile mice. (A) Mice were microinjected with AAVs (P60: AAV-iC++ or AAV-GFP, P20: AAV-NpACY or AAV-GFP), trained in contextual fear conditioning, then tested the next day in Context A or B with no light followed by blue (iC++) or red (NpACY) light to silence CA1 pyramidal neurons. **(B)** iC++ and NpACY viral expression in CA1 of P60 and P20 mice. **(C)** Silencing CA1 pyramidal neurons during testing impaired memory retrieval for P20 and P60 mice in Context A (RM-ANOVA, main effect of Light: $F_{1,13} = 62.74$, $P < 10^{-5}$) and P20 mice in Context B (RM-ANOVA, Age × Light interaction: $F_{1,14} = 28.80$, $P < 0.0001$). **(D)** Red and blue light alone do not impair memory recall in P20 and P60 mice, respectively, in Context A (RM-ANOVA, $P > 0.05$) or Context B (RM-ANOVA, main effect of Age: $F_{1,13} = 34.14$, $P < 0.0001$). **(E)** Mice were microinjected with AAV-iC++ or AAV-GFP, trained in contextual fear conditioning on P20, then tested the next day in Context A with no light followed by blue light to silence CA1 pyramidal neurons. **(F)** Blue light non-specifically reduced freezing behavior in P20 mice during the test (RM-ANOVA, main effect of Light: $F_{1,6} = 118.38$, $P < 0.0001$). Data points are individual mice with mean ± s.e.m. Scale bars: yellow = 500 μm. *** $P < 0.001$.

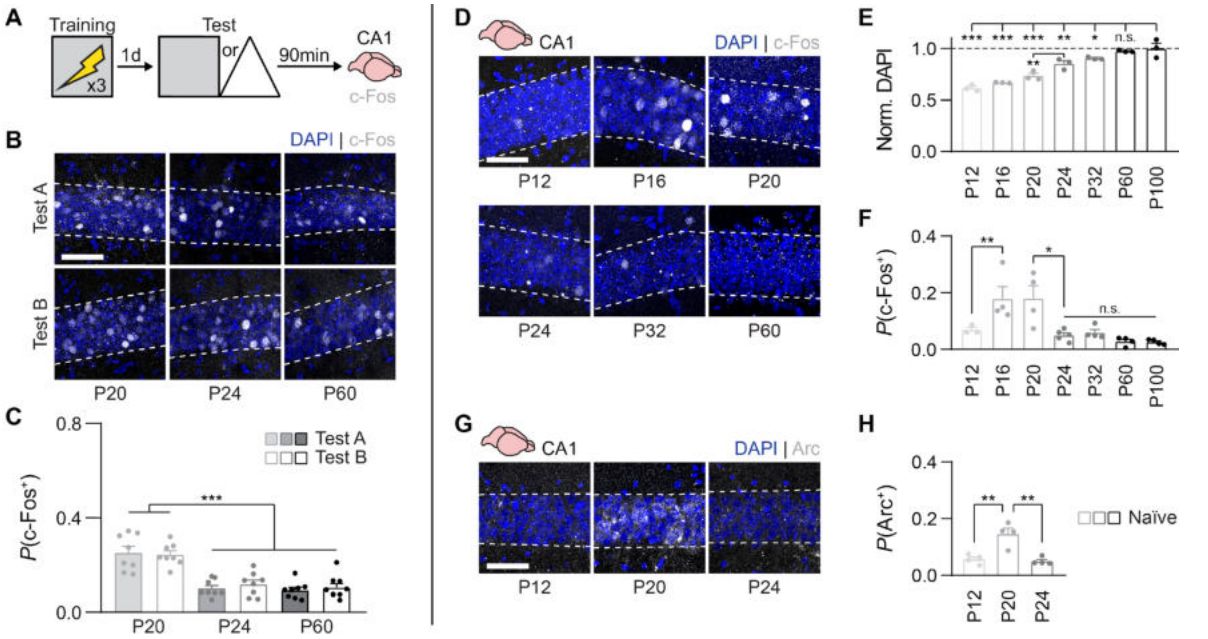

Figure S4. Immediate-early gene expression is transiently elevated in CA1 during the third postnatal week (Related to Figure 1). (A) Mice were trained in contextual fear conditioning, and c-Fos expression in dorsal CA1 was examined 90-min after the tests in Contexts A or B **(B)** c-Fos expression in CA1 pyramidal layer after contextual fear retrieval. **(C)** After testing, the proportion of pyramidal layer cells expressing c-Fos was elevated in P20 mice compared to P24 and P60 mice (ANOVA, main effect of Age: $F_{2,43} = 43.30$, $P < 10^{-6}$). **(D)** c-Fos expression in CA1 pyramidal layer cells across development. **(E)** The density of DAPI^{+} cells in CA1 (normalized to the mean of mature adults, P100) increased into adulthood (ANOVA, main effect of Age: $F_{6,14} = 34.42$, $P < 10^{-6}$). **(F)** The proportion of pyramidal layer cells expressing c-Fos was elevated in naive 'home cage' mice during the third postnatal week (P16 to P20) (ANOVA, main effect of Age: $F_{6,21} = 7.30$, $P < 0.001$). **(G)** Arc expression in CA1 pyramidal layer cells across early development. **(H)** The proportion of pyramidal later cells expressing Arc was elevated in naive 'home cage' mice during the third postnatal week (P20) (ANOVA, main effect of Age: $F_{2,9} = 15.75$, $P < 0.01$). Data points are individual mice with mean ± s.e.m. Scale bars: white = 50 μm. * $P < 0.05$; ** $P < 0.01$; *** $P < 0.001$.

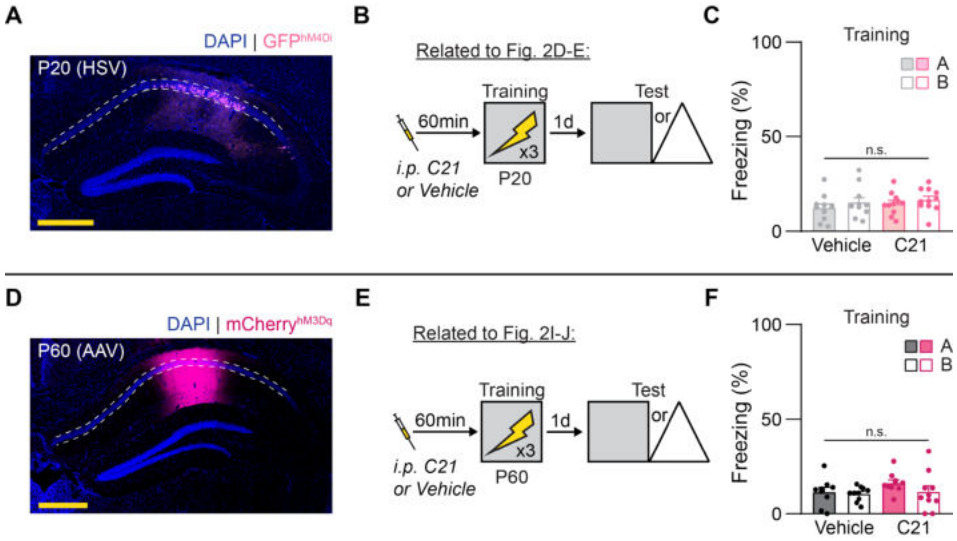

Figure S5. Chemogenetic manipulation of pyramidal neurons training data (Related to Figure 2). (A) hM4Di expression in dorsal CA1 of a P20 mouse. **(B to C)** Injecting P20 mice with C21 before training (B) did not alter freezing behavior during training (C, ANOVA, $P > 0.05$). **(D)** hM3Dq expression in dorsal CA1 of a P60 mouse. **(E to F)** Injecting P60 mice with C21 before training (E) did not alter freezing behavior during training (F, ANOVA, $P > 0.05$). Data points are individual mice with mean ± s.e.m. Scale bars: yellow = 500 μm.

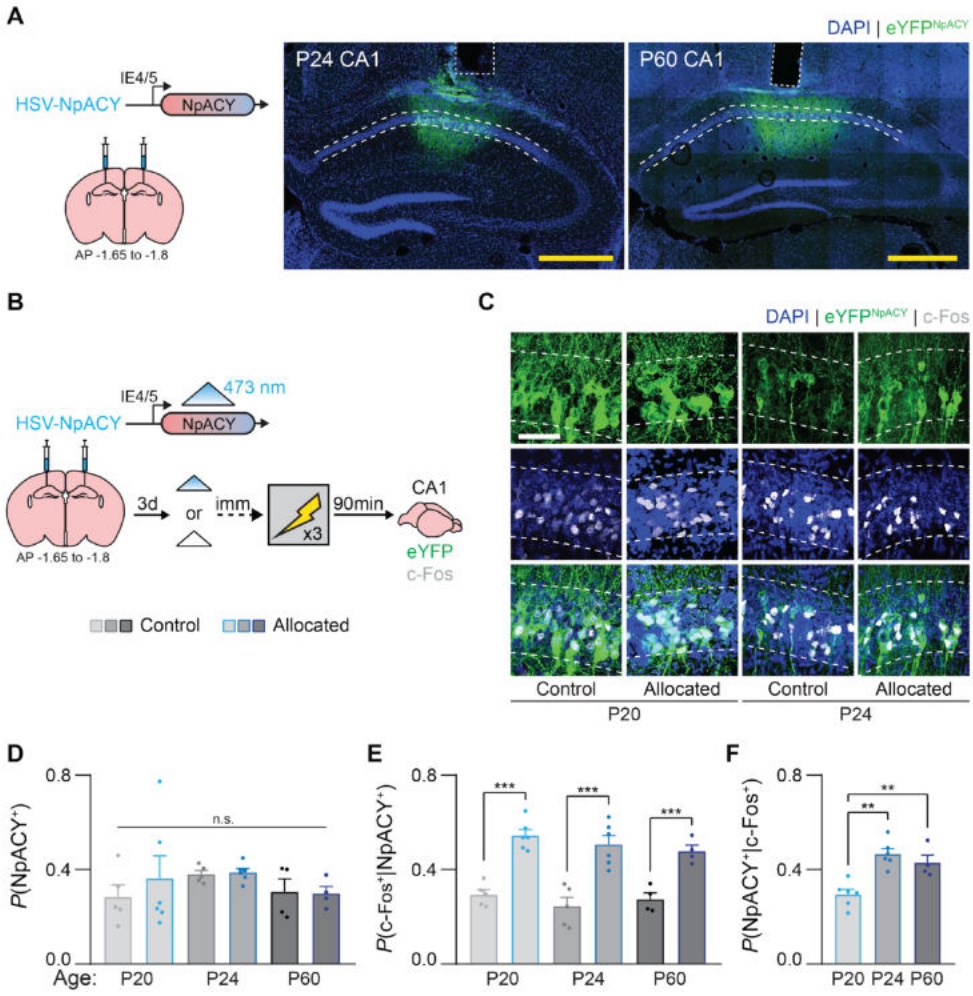

Figure S6. Optogenetics-mediated neuronal allocation in CA1 is effective regardless of mouse age (Related to Figure 3). (A) HSV-NpACY expression in dorsal CA1 of P24 and P60 mice. **(B)** Mice were microinjected with HSV-NpACY in CA1 and three days later, blue light or no light was delivered for 30 s immediately before contextual fear conditioning training. c-Fos expression was examined 90-min after training. **(C)** NpACY and c-Fos expression in dorsal CA1. **(D to F)** The proportion of neurons expressing HSV-NpACY did not differ across groups (D, ANOVA, $P > 0.05$). Blue-light stimulation immediately before training resulted in greater c-Fos expression in NpACY^{+} neurons in all age groups (E, ANOVA, main effect of Light: $F_{1,24} = 86.88$, $P < 10^{-6}$), but c-Fos was expressed in more NpACY^{-} neurons in P20 mice compared with P24 and P60 mice (F, ANOVA, main effect of Age: $F_{2,13} = 14.17$, $P < 0.001$). Data points are individual mice with mean ± s.e.m. Scale bars: white = 50 μm, yellow = 500 μm. * $P < 0.05$; ** $P < 0.01$; *** $P < 0.001$.

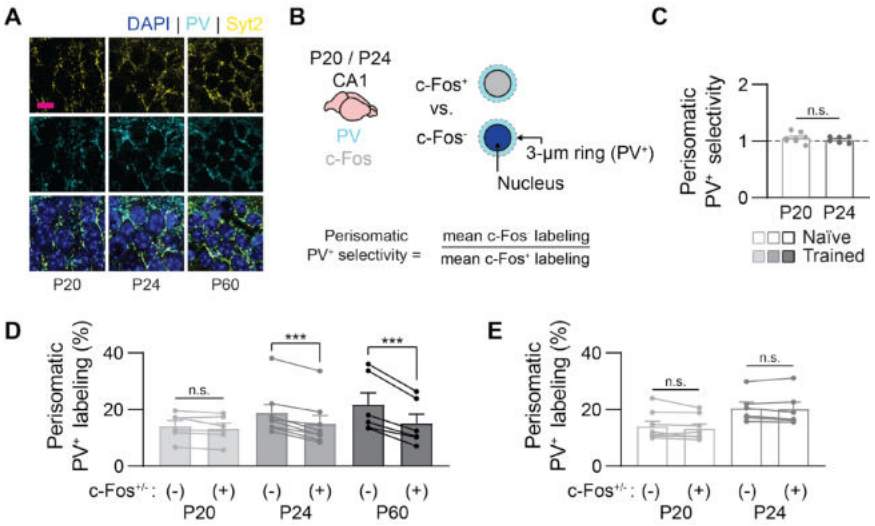

Figure S7. Perisomatic PV$^+$ selectivity in experimentally naïve mice (Related to Figure 4). **(A)** Co-localization of Syt2$^+$ synaptic puncta and PV$^+$ neurites across development. **(B)** Perisomatic PV$^+$ selectivity analysis was performed on CA1 pyramidal layer cells from naive P20 and P24 mice as a negative control. **(C)** PV$^+$ neurite selectivity did not increase with age in experimentally naïve mice (unpaired *t*-test, $t_{12} = 0.72$, $P = 0.48$). **(D)** PV$^+$ neurites were selectively localized around c-Fos$^-$ compared to c-Fos$^+$ cells in P24 and P60, but not P20, mice after conditioning (RM-ANOVA, Age × c-Fos interaction: $F_{2,17} = 15.71$, $P < 0.001$). **(E)** PV$^+$ neurites were not selectively localized around c-Fos$^-$ compared to c-Fos$^+$ cells in experimentally naïve mice (RM-ANOVA, main effect of Age: $F_{1,12} = 6.09$, $P < 0.05$). Data points are individual mice with mean ± s.e.m. Scale bars: magenta = 10 μm. *** $P < 0.001$.

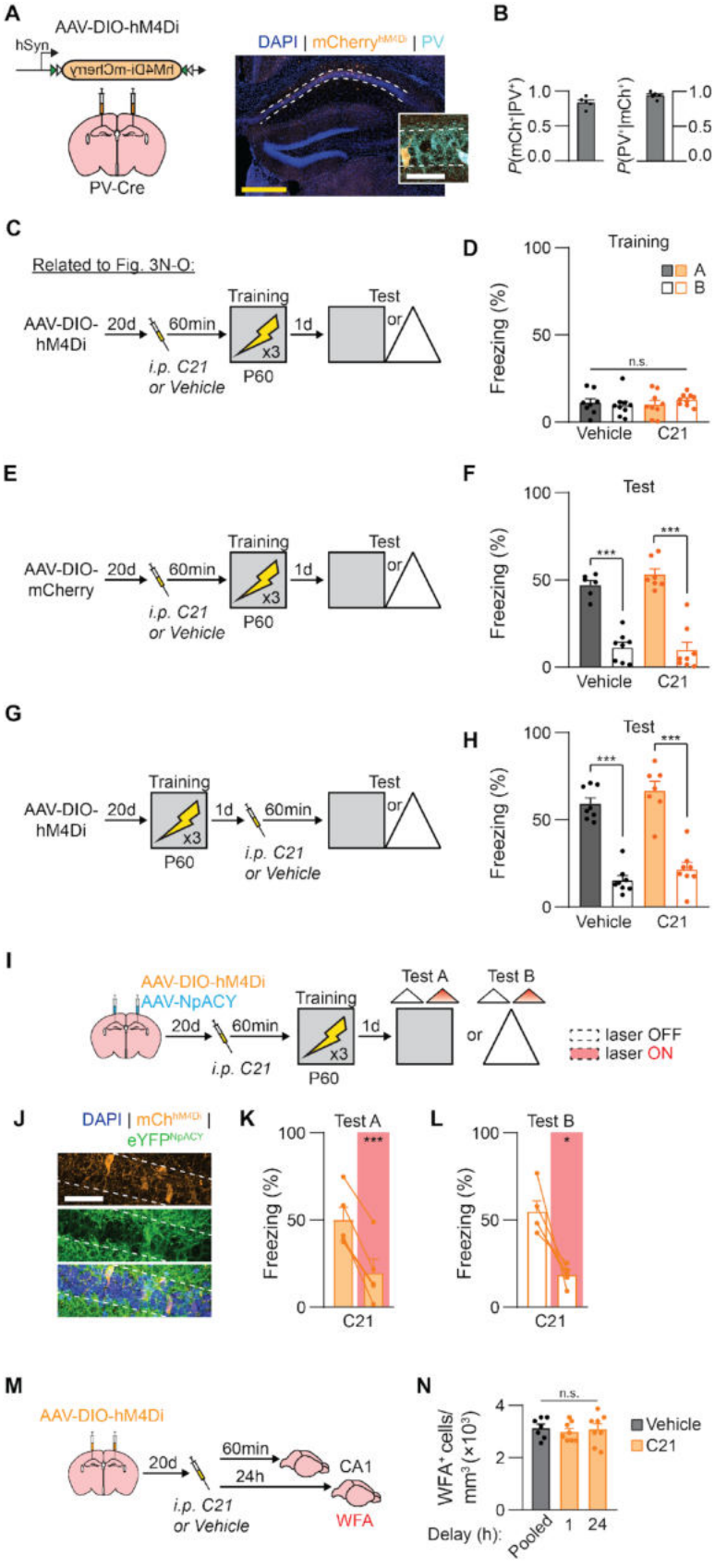
A
AAV-DIO-hM4Di
hSyn
PV-Cre
DAPI | mCherry^hM4Di | PV
B
P(mCh+|PV+)
P(PV+|mCh+)
1.0
0.5
0.0
C
Related to Fig. 3N-O:
AAV-DIO-hM4Di
20d
60min
i.p. C21 or Vehicle
Training
x3
P60
1d
Test
or
D
Training
A
B
Freezing (%)
n.s.
Vehicle
C21
E
AAV-DIO-mCherry
F
***
G
AAV-DIO-hM4Di
H
I
AAV-DIO-hM4Di
AAV-NpACY
i.p. C21
Test A
Test B
laser OFF
laser ON
J
DAPI | mCh^hM4Di | eYFP^NpACY
K
L
M
AAV-DIO-hM4Di
24h
CA1
WFA
N
WFA+ cells/mm3 (×10^3)
Delay (h):
Pooled
1
24

Figure S8. Control experiments for using chemogenetics to inhibit CA1 PV$^+$ interneurons (Related to Figure 4). (A to B) AAV-DIO-hM4Di was expressed in dorsal CA1 (A) resulting in high penetrance (left) and specificity (right) of hM4Di in PV$^+$ cells (B). **(C to D)** Injecting P60 PV::hM4Di mice with C21 before training (C) did not alter freezing behavior during training (D, ANOVA, $P > 0.05$). **(E to F)** Injecting P60 PV::mCherry mice with C21 before training (E) did not alter memory precision (F, main effect of Test Context: $F_{1,25} = 123.31$, $P < 10^{-6}$). **(G to H)** Injecting PV::hM4Di mice with C21 before testing (G) did not alter memory precision (H, ANOVA, main effect of Test Context: $F_{1,27} = 134.56$, $P < 10^{-6}$). **(I to L)** Mice were microinjected with AAV-DIO-hM4Di and AAV-NpACY in dorsal CA1, injected with C21 1-h before training, then tested the next day in Context A or Context B without and with red light to silence CA1 pyramidal neurons (I). hM4Di expression in CA1 PV$^+$ interneurons and NpACY in CA1 excitatory neurons (J). Inhibiting CA1 PV$^+$ interneurons before training in P60 mice resulted in hippocampus-dependent imprecise memories. Silencing CA1 neurons with red light reduced freezing in Context A (K, paired *t*-test: $t_4 = 9.77$, $P < 0.001$) and in Context B (L, paired *t*-test: $t_4 = 4.30$, $P < 0.05$). **(M to N)** Adult PV-Cre mice were microinjected with AAV-DIO-hM4Di in dorsal CA1, injected with C21, and WFA expression in dorsal CA1 was examined 1 or 24 h later (M). Acute PV$^+$ interneuron inhibition did not alter WFA$^+$ PNN density at timepoints relevant to contextual fear conditioning training or testing (N, ANOVA, $P > 0.05$). Data points are individual mice with mean ± s.e.m. Scale bars: white = 50 μm, yellow = 500 μm. * $P < 0.05$; ** $P < 0.01$; *** $P < 0.001$.

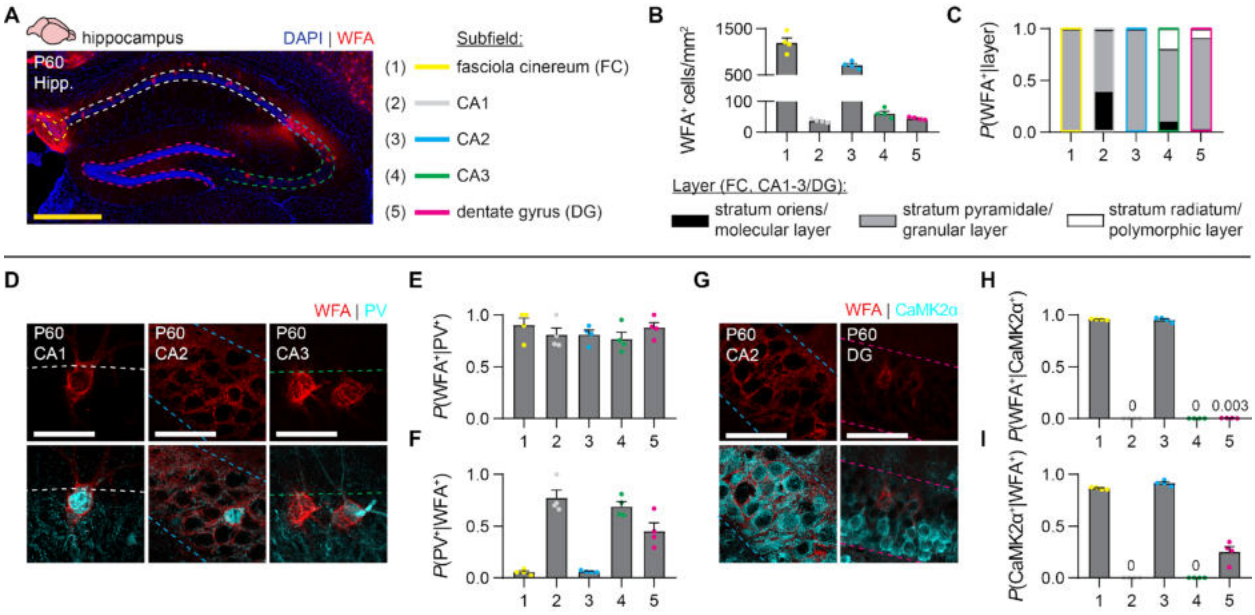

Figure S9. Characterization of PNNs in the adult mouse dorsal hippocampus.

(A) PNNs were identified in the P60 dorsal hippocampus using WFA staining. **(B)** WFA^+ PNNs were sparsely distributed in subfields CA1, CA3, and dentate gyrus (DG), and densely packed in fasciola cinereum (FC) and CA2. **(C)** Across all subfields, most WFA^+ PNNs were located in the pyramidal/granule cell layer. **(D)** Colocalization of WFA^+ PNNs with PV^+ interneurons in different subfields. **(E)** The majority of PV^+ interneurons in the dorsal hippocampus were surrounded by WFA^+ PNNs. **(F)** A minority WFA^+ PNNs surrounded PV^- cells in CA1 and CA3, and to a lesser extent in DG. **(G)** Colocalization of WFA^+ PNNs with $CaMK2\alpha^+$ excitatory neurons in different subfields. **(H)** The majority $CaMK2\alpha^+$ neurons in FC and CA2 were surrounded by WFA^+ PNNs, and no $CaMK2\alpha^+$ neurons in CA1 and CA3 were surrounded by WFA^+ PNNs. A small proportion of $CaMK2\alpha^+$ neurons (likely, mature granule cells based on proximity to the hilus) were surrounded by WFA^+ PNNs. **(I)** A minority WFA^+ PNNs surrounded $CaMK2\alpha^-$ cells in FC and CA2. Data points are individual mice with mean ± s.e.m. Scale bars: white = 50 μm, yellow = 500 μm.

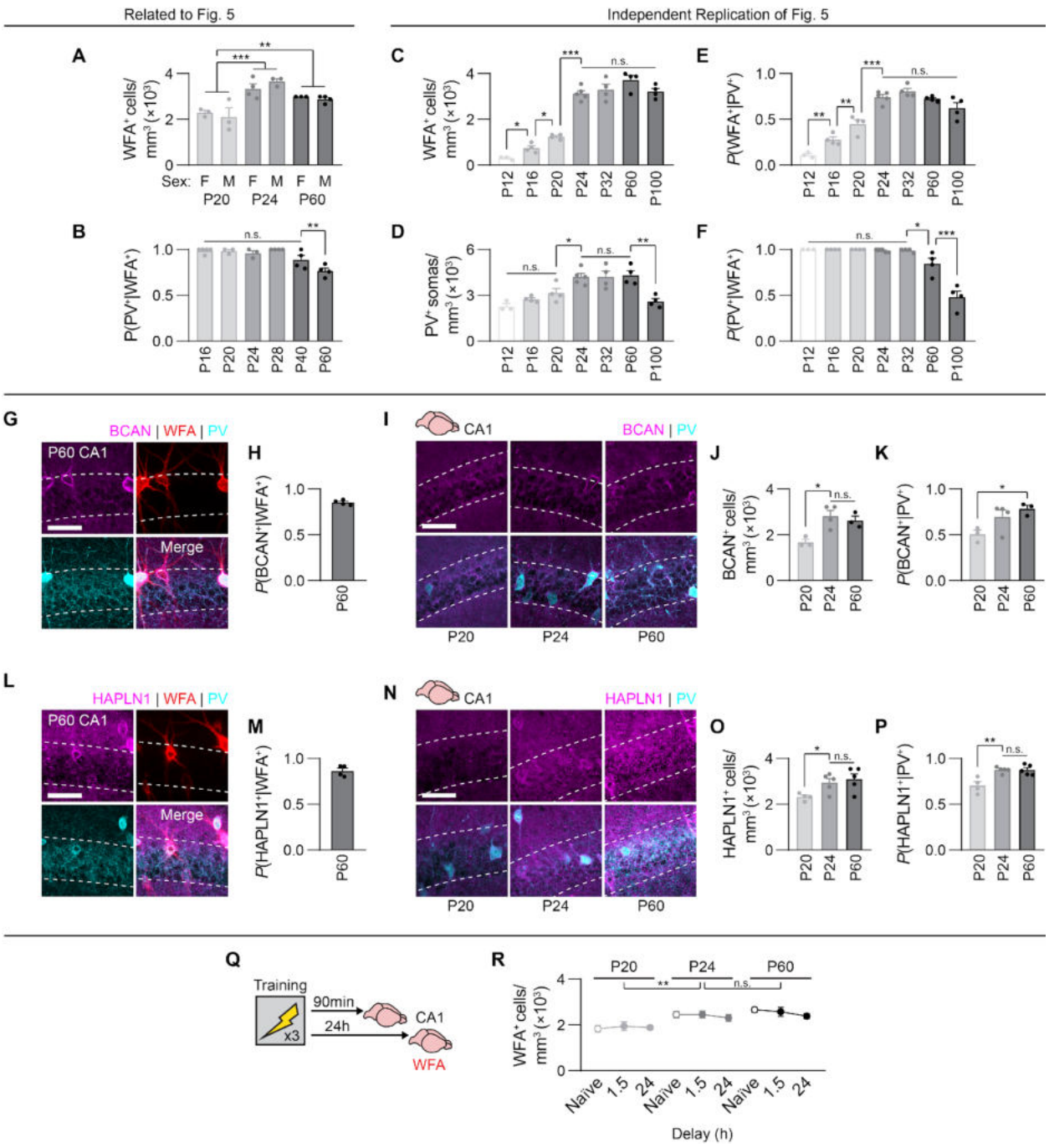

Figure S10. Maturation of CA1 PNNs (Related to Figure 5). (A) The maturation of CA1 PNNs by P24 was not sex-dependent (ANOVA, main effect of Age: $F_{2,14} = 22.13$, $P < 0.0001$). **(B)** A small proportion of WFA^+ PNNs surrounding PV^- cells form in CA1 during young adulthood (ANOVA, main effect of Age: $F_{5,17} = 10.94$, $P < 0.0001$). **(C to F)** Independent replication of Figure 5C-D with expanded Age range. The density of WFA^+ PNNs (C, ANOVA, main effect of Age: $F_{6,21} = 82.50$, $P < 10^{-6}$), PV^+ interneurons (D, ANOVA, main effect of Age: $F_{6,21} = 10.70$, $P < 0.0001$), and proportion of PV^+ interneurons surrounded by WFA^+ PNNs (E, ANOVA, main effect of Age: $F_{6,21} = 46.68$, $P < 10^{-6}$) reach adult-like levels by P24, with WFA^+PV^- PNNs developing during adulthood (F, ANOVA, main effect of Age: $F_{6,21} = 32.30$, $P <$

10^{-6}). **(G to H)** High colocalization of BCAN with WFA^+ PNNs in P60 CA1. **(I to K)** Increased density of $BCAN^+$ cells (J, ANOVA, main effect of Age: $F_{2,7} = 8.40$, $P < 0.05$) and colocalization of BCAN and PV^+ interneurons (K, ANOVA, main effect of Age: $F_{2,7} = 4.70$, $P = 0.05$) across development in dorsal CA1. **(L to M)** High colocalization of HAPLN1 with WFA^+ PNNs in P60 CA1. **(N to P)** Increased density of $HAPLN1^+$ cells (O, ANOVA, main effect of Age: $F_{2,11} = 4.55$, $P < 0.05$) and colocalization of HAPLN1 and PV^+ interneurons (P, ANOVA, main effect of Age: $F_{2,11} = 12.05$, $P < 0.01$) across development in dorsal CA1. **(Q to R)** WFA expression in dorsal CA1 was examined 90-min or 24-h after contextual fear conditioning (Q). Training did not alter the trajectory of WFA^+ PNN development in CA1 (R, ANOVA, main effect of Age: $F_{2,52} = 5.88$, $P < 0.01$). Data points are individual mice with mean ± s.e.m. Scale bars: white = 50 μm. * $P < 0.05$; ** $P < 0.01$; *** $P < 0.001$.

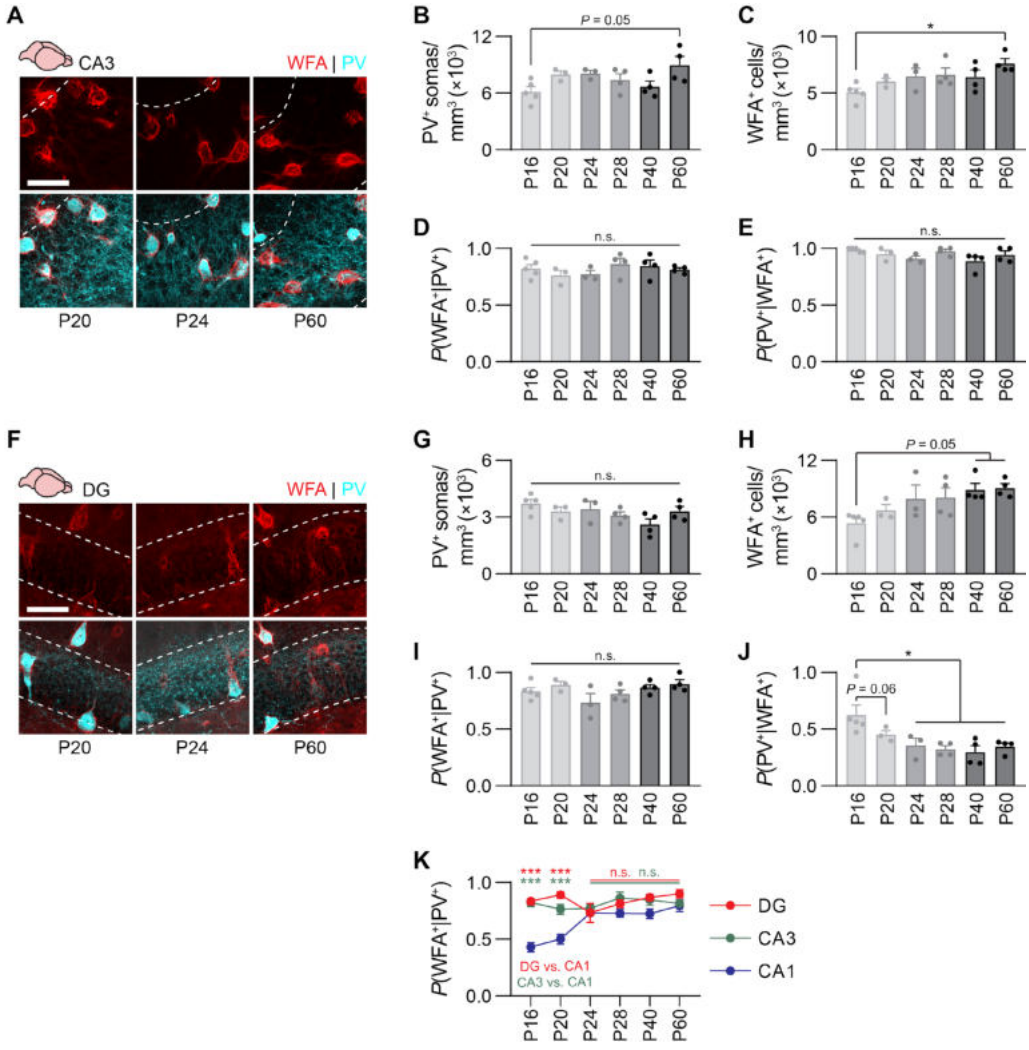

Figure S11. Maturation of CA3 and DG PNNs (Related to Figure 5). (A) WFA$^+$ PNNs surrounding PV$^+$ interneurons in CA3 across development. **(B to E)** In CA3, the density of PV$^+$ interneurons (B, ANOVA, main effect of Age: $F_{5,17} = 2.87$, $P < 0.05$) and WFA$^+$ PNNs (C, ANOVA, main effect of Age: $F_{5,17} = 3.17$, $P < 0.05$) increased slightly between P16 and P60. The proportion of PV$^+$ interneurons surrounded by WFA$^+$ PNNs reached adult-like levels before P16 (D, ANOVA, $P > 0.05$), and there was no further development of WFA$^+$ PNNs around PV$^-$ cells from P16 to P60 (E, ANOVA, $P > 0.05$). **(F)** WFA$^+$ PNNs surrounding PV$^+$ interneurons in DG across development. **(G to J)** In DG, the density of PV$^+$ interneurons did not change (G, ANOVA, $P > 0.05$) and WFA$^+$ PNNs increased (H, ANOVA, main effect of Age: $F_{5,17} = 3.46$, $P < 0.05$) between P16 and P60. The proportion of PV$^+$ interneurons surrounded by WFA$^+$ PNNs reached adult-like levels before P16 (I, ANOVA, $P > 0.05$), and WFA$^+$ PNNs around PV$^-$ cells increased from P16 to P60 (J, ANOVA, main effect of Age: $F_{5,17} = 4.85$, $P < 0.01$). **(K)** Development of WFA$^+$ PNNs around PV$^+$ interneurons were delayed in CA1 compared to CA3 and DG (RM-ANOVA, Age × Region interaction: $F_{10,34} = 7.42$, $P < 10^{-5}$). Data shown in Panel S11K are re-plotted from Fig. 4D, S11D, and S11I, and re-analyzed. Data points are individual mice with mean ± s.e.m. Scale bars: white = 50 μm. * $P < 0.05$.

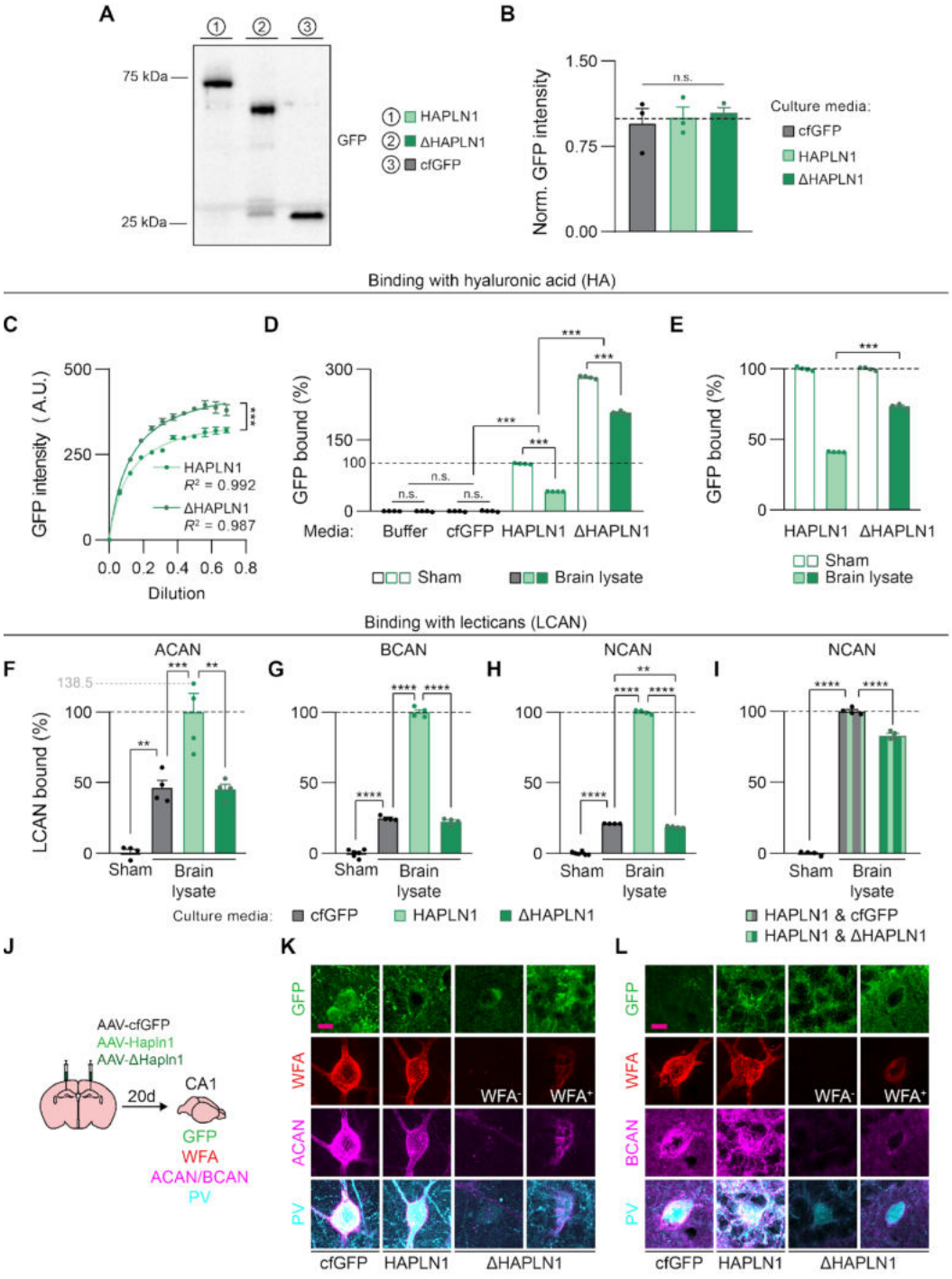

Figure S12. ΔHAPLN1 is a dominant-negative isoform of HAPLN1 that does not bind lecticans (Related to Figure 5). (A-B) Prediluted samples of HAPLN1-enriched culture media contained the same amount of GFP (B, ANOVA, $P > 0.05$). **(C-E)** ΔHAPLN1 more strongly interacted with hyaluronic acid (HA) than full HAPLN1. Non-linear fitting of the data showed that binding curves for ΔHAPLN1 and HAPLN1 differed significantly (C, ΔAIC = 138.4, $P < 0.0001$), with ΔHAPLN1 having a higher saturation level (B_{max} = 467.9, 95% CI [455.6, 480.8]) compared with full HAPLN1 (B_{max} = 380.1, 95% CI [369.5, 391.2]; ΔAIC = 49.69, $P < 0.0001$), but not higher binding affinity (ΔAIC = -1.4, P = 0 .6682), therefore the shared dissociation

constant was used for fitting (K_d = 0.1183, 95% CI [0.1073, 0.1302]). **(D-E)** Compared to full HAPLN1, ΔHAPLN1 more strongly bound to HA in the presence or absence of lectican (LCAN)-containing brain lysate (D, ANOVA, Media × Brain interaction: $F_{3,24} = 677.88$, $P < 10^{-5}$; Data normalized from 0% [Buffer wells] to 100% [HAPLN1 and Sham (1% BSA TBST) wells]) and was less easily displaced by brain lysate (E, ANOVA, Media × Brain interaction: $F_{1,12} = 721.07$, $P < 10^{-7}$; Data normalized to 100% [respective Sham wells]). **(F-H)** Full HAPLN1, but not ΔHAPLN1, enhanced binding of aggrecan (ACAN; F, ANOVA, main effect of Media: $F_{3,12} = 23.63$, $P < 0.0001$), brevican (BCAN; G, main effect of Media: $F_{3,14} = 1158$, $P < 0.0001$), and neurocan (NCAN; H, main effect of Media: $F_{3,14} = 8755$, $P < 0.0001$) to HA. Data normalized from 0% (Sham wells) to 100% (HAPLN1 and Brain lysate wells). **(I)** ΔHAPLN1 impaired binding of NCAN to HA in the presence of full HAPLN1 (ANOVA, $F_{2,9} = 2098$, $P < 0.0001$). Data normalized from 0% (Sham wells) to 100% (HAPLN1-cfGFP and Brain lysate wells). **(J-L)** Overexpression of ΔHAPLN1 in the CA1 of adult mice (J) impaired binding of ACAN (K) and BCAN (J) around parvalbumin-expressing interneurons. Data points are technical replicates with mean ± s.e.m. Scale bars: magenta = 10 μm. ** $P < 0.01$; *** $P < 0.001$; **** $P < 0.0001$.

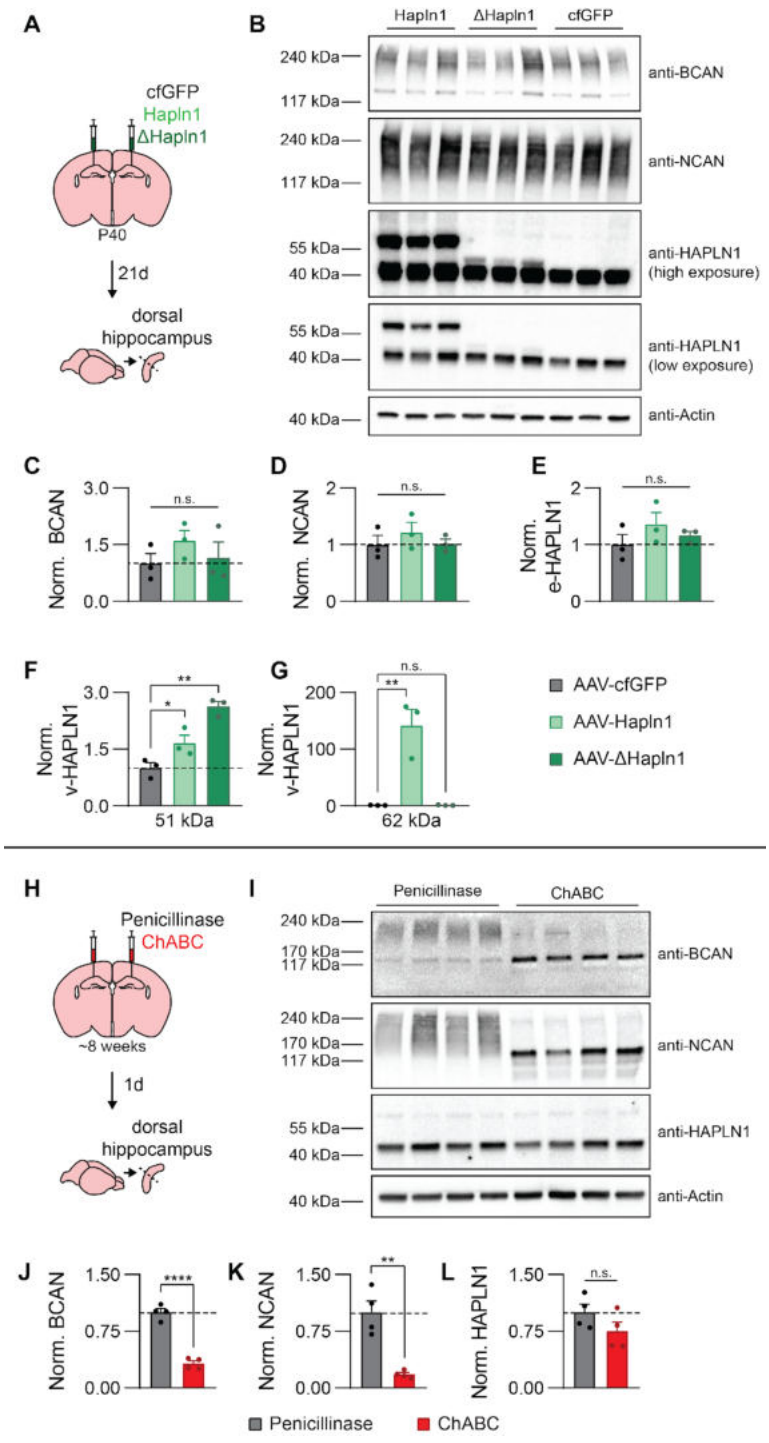

Figure S13. Viral overexpression of HAPLN1 or ΔHAPLN1 does not alter endogenous lectican or HAPLN1 expression (Related to Figure 5). (A) Mice were microinjected with AAV-cfGFP, AAV-Hapln1, or AAV-ΔHapln1 in the dorsal hippocampus. Three weeks later, hippocampi of adult mice were dissected and used for western blot analyses of glycosylated lecticans and HAPLN1. **(B)** Western blot illustrating changes in endogenous brevican (BCAN), neurocan (NCAN), HAPLN1 (e-HAPLN1), and virally expressed HAPLN1 (v-HAPLN1) in

dorsal hippocampus extracts following AAV expression. Actin was used as a loading control. Individual lanes are different mice. **(C to G)** AAV-Hapln1 and AAV-ΔHapln1 did not alter BCAN (C, ANOVA, $P > 0.05$), NCAN (D, ANOVA, $P > 0.05$), or e-HAPLN1 (E, ANOVA, $P > 0.05$) expression, but increased v-HAPLN1 expression (F, 51 kDa: ANOVA, main effect of Virus: $F_{2,6} = 24.71$, $P < 0.01$; G, 62 kDa: ANOVA, main effect of Virus: $F_{2,6} = 23.40$, $P < 0.01$). **(H)** Mice were microinjected with Penicillinase or ChABC in the dorsal hippocampus. One day later, hippocampi of adult mice were dissected and used for western blot analyses. **(I)** Western blot illustrating changes in endogenous BCAN, NCAN, HAPLN1 in dorsal hippocampus extracts following enzyme injection. Actin was used as a loading control. Individual lanes are different mice. **(J to L)** ChABC treatment reduced BCAN (J, unpaired *t*-test: $t_6 = 11.23$, $P < 0.0001$), NCAN (K, unpaired *t*-test: $t_6 = 5.41$, $P < 0.01$), but not HAPLN1 (L, unpaired *t*-test: $t_6 = 1.53$, $P = 0.17$) in dorsal hippocampus. Data points are individual mice with mean ± s.e.m. Data are normalized to the mean of the control group (AAV-cfGFP or Penicillinase). * $P < 0.05$; ** $P < 0.01$; *** $P < 0.001$; **** $P < 0.0001$.

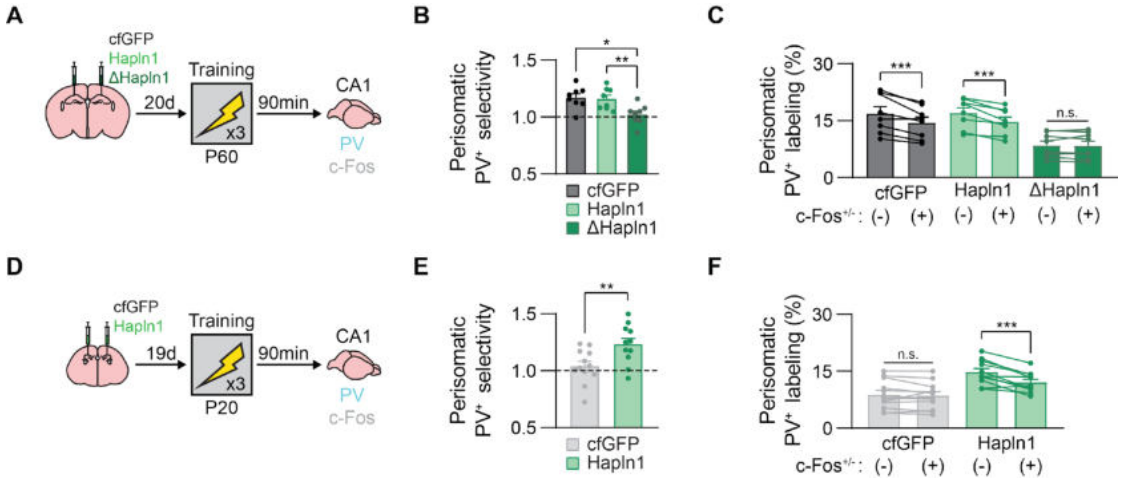

Figure S14. Maturation of CA1 PNNs is necessary and sufficient for learning-related structural plasticity of PV$^+$ neurites (Related to Figure 6). (A to C) Mice were microinjected with AAV-cfGFP, AAV-Hapln1, or AAV-ΔHapln1 in the dorsal CA1 and trained in contextual fear conditioning on P60. Localization of PV$^+$ neurites was analyzed around c-Fos$^-$ and c-Fos$^+$ nuclei 90 min after training (A). PV$^+$ neurites were selectively localized around c-Fos$^-$ compared to c-Fos$^+$ cells in mice expressing AAV-cfGFP and AAV-Hapln1, but not AAV-ΔHapln1, (B, ANOVA, main effect of Virus: $F_{2,21} = 6.38$, $P < 0.01$; C, RM-ANOVA, Virus × c-Fos interaction: $F_{2,21} = 8.84$, $P < 0.01$). **(D to F)** Mice were microinjected with AAV-cfGFP or AAV-Hapln1 in the dorsal CA1 and trained in contextual fear conditioning on P20. Localization of PV$^+$ neurites was analyzed around c-Fos$^-$ and c-Fos$^+$ nuclei 90 min after training (D). PV$^+$ neurites were selectively localized around c-Fos$^-$ compared to c-Fos$^+$ cells in mice expressing AAV-Hapln1 but not AAV-cfGFP, (E, unpaired *t*-test: $t_{21} = 2.86$, $P < 0.01$; C, RM-ANOVA, Virus × c-Fos interaction: $F_{1,21} = 13.72$, $P < 0.01$). Data points are individual mice with mean ± s.e.m. * $P < 0.05$; ** $P < 0.01$; *** $P < 0.001$.

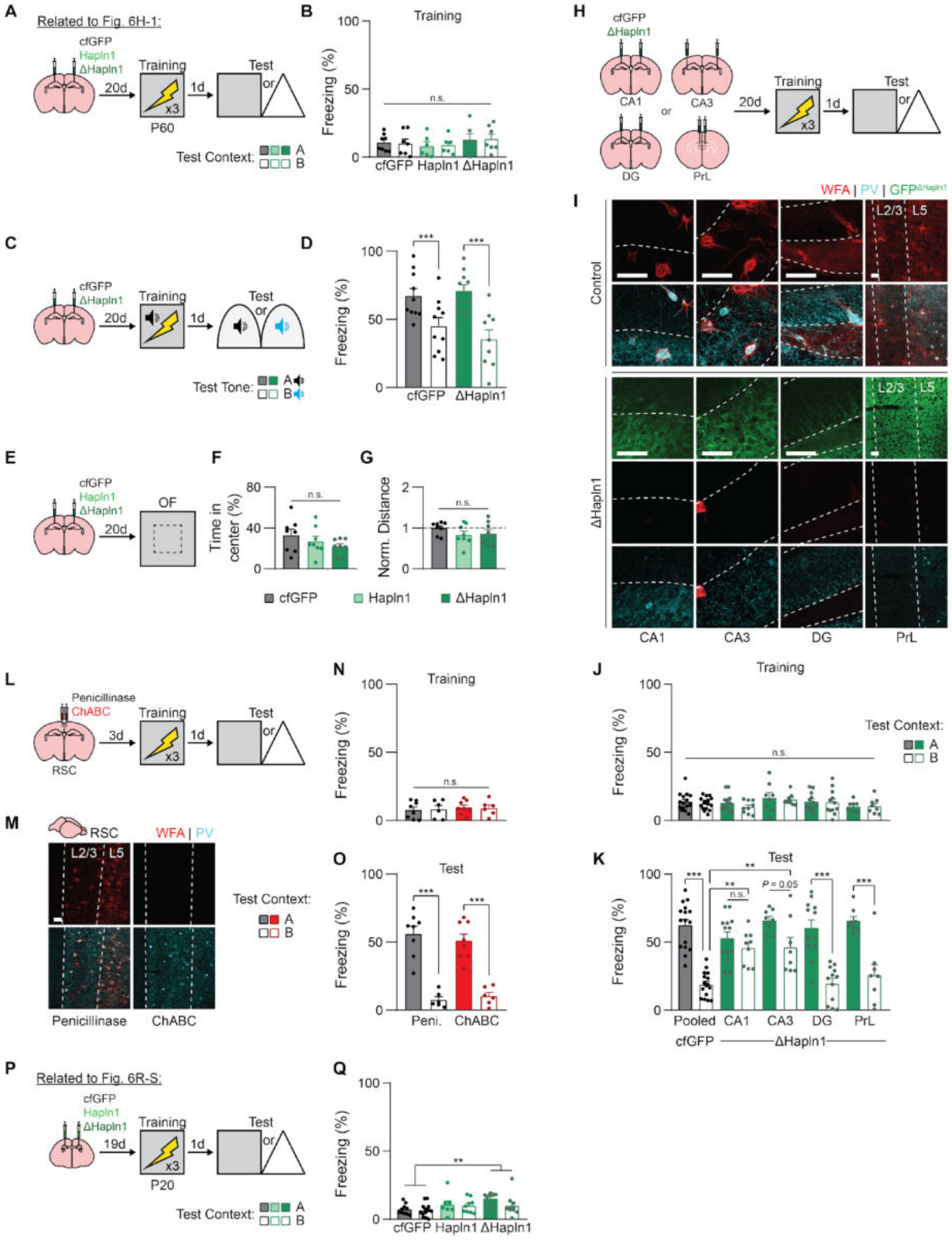

Figure S15. Hippocampal (and not cortical) PNNs are necessary for contextual memory precision in adult mice (Related to Figure 6). (A to B) Expression of AAV-Hapln1 or AAV-ΔHapln1 in the dorsal CA1 (A) did not alter P60 mouse freezing behavior during training

(B, ANOVA, $P > 0.05$). **(C to D)** Expression of AAV-ΔHapln1 in the dorsal CA1 before tone fear conditioning (C) did not alter memory precision for similar auditory cues (D, ANOVA, main effect of Test Tone: $F_{1,35} = 24.68$, $P < 0.0001$). **(E to G)** Expression of AAV-Hapln1 or AAV-ΔHapln1 in the dorsal CA1 before an open field test (E) did not alter anxiety-like behavior (F, ANOVA, $P > 0.05$) or locomotion (G, ANOVA, $P > 0.05$) in adult mice. **(H to K)** Expression of AAV-ΔHapln1 in CA1, CA3, or DG of the hippocampus, or the prelimbic region (PrL) of the medial prefrontal cortex before contextual fear conditioning (H) destabilized PNNs in the corresponding brain region (I) but did not alter freezing behavior during training (J, ANOVA, $P > 0.05$). Destabilizing PNNs in CA1 or CA3 (but not DG or PrL) with AAV-ΔHapln1 reduced memory precision in adult mice during the memory test (K, ANOVA, Virus/Region × Test Context interaction: $F_{4,100} = 5.84$, $P < 0.001$). **(L to O)** Microinjection of ChABC into the retrosplenial cortex (RSC) before contextual fear conditioning (L) digested PNNs (M) and did not alter freezing behavior during training (N, ANOVA, $P > 0.05$) or during the memory test (O, ANOVA, main effect of Test Context: $F_{1,24} = 92.64$, $P < 10^{-6}$). **(P to Q)** Expression of AAV-Hapln1 in the dorsal CA1 (P) did not alter P20 mouse freezing behavior during training (Q, ANOVA, main effect of Virus: $F_{2,53} = 5.17$, $P < 0.01$). Data points are individual mice with mean ± s.e.m. Scale bars: white = 50 μm. * $P < 0.05$; ** $P < 0.01$; *** $P < 0.001$.

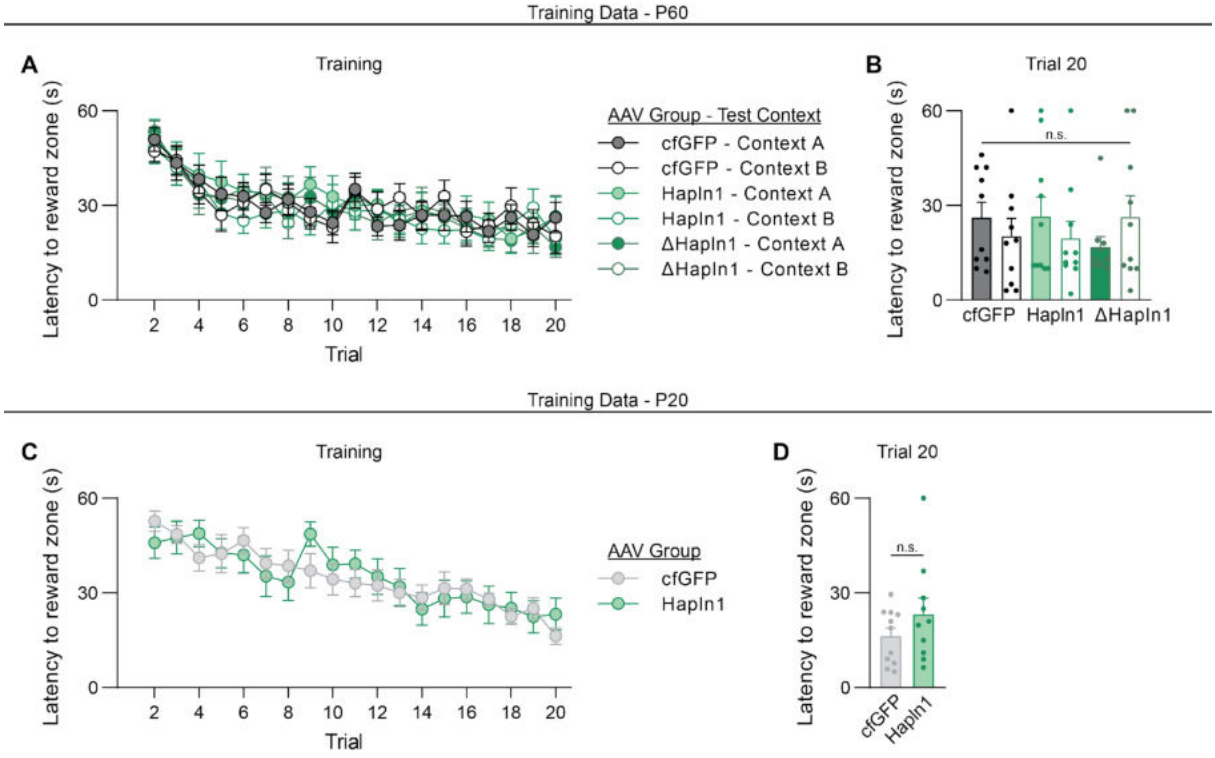

Figure S16. Spatial foraging task training data for mice with viral PNN manipulations (Related to Figure 6). (A to B) In adult mice, latencies to locate the reward zone decreased across training trials in all groups (A) and did not differ across groups by the last training trial (B, ANOVA, $P > 0.05$). **(C to D)** In juvenile mice, latencies to locate the reward zone decreased across training trials in both groups (C) and did not differ between groups by the last training trial (D, unpaired *t*-test: $t_{19} = 1.26$, $P = 0.22$). Data points are individual mice with mean ± s.e.m.

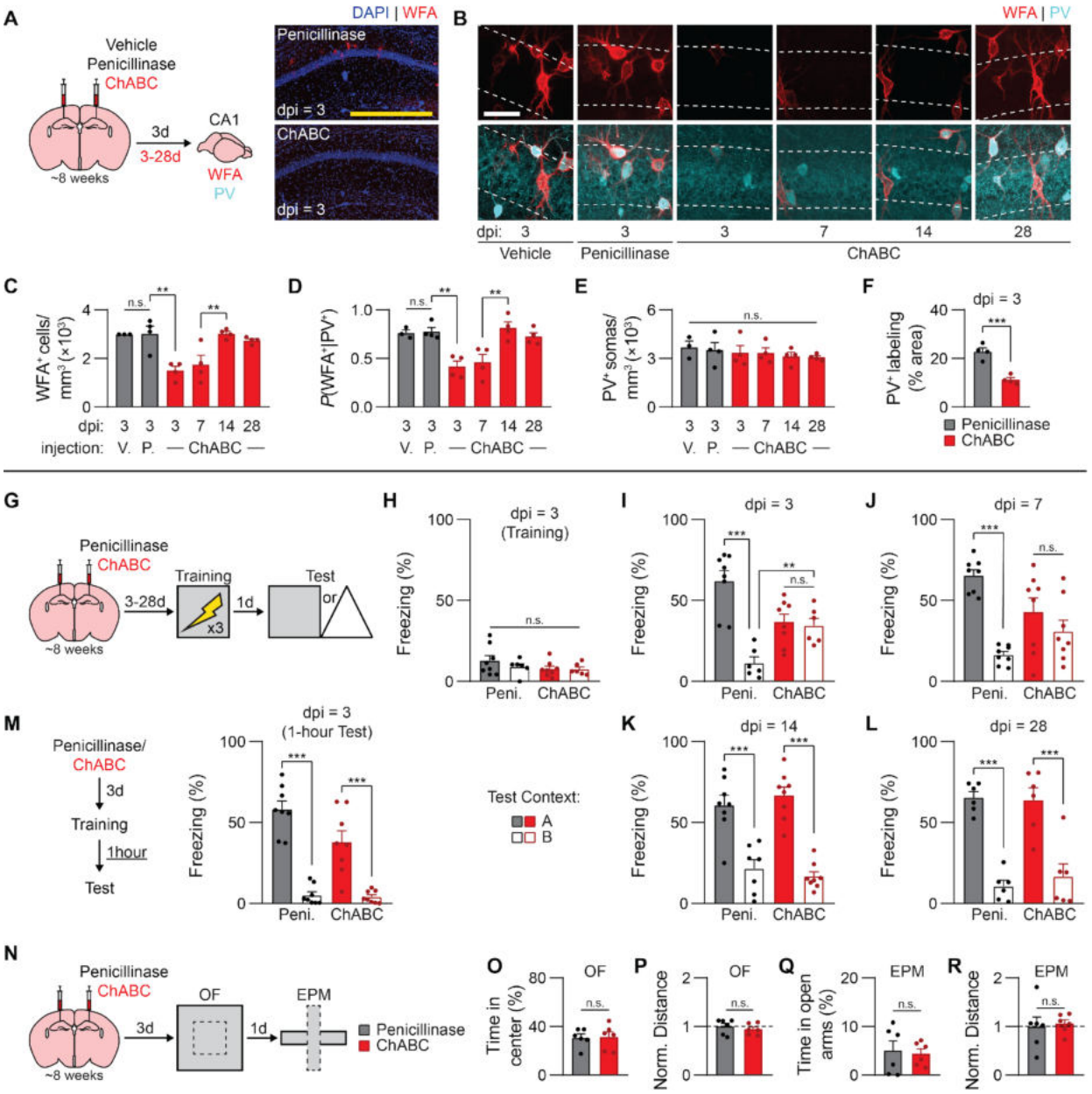

Figure S17. Enzymatic digestion of CA1 PNNs with ChABC reinstates juvenile-like memory imprecision. (A) Chondroitinase ABC (ChABC) was microinjected into the dorsal CA1 of adult mice to rapidly digest PNNs, and mice were perfused 3-28 d post-injection (dpi). **(B)** WFA^+ PNNs and PV^+ interneurons in dorsal CA1 at different dpi. **(C to F)** ChABC treatment transiently reduced the density of WFA^+ PNNs (C, ANOVA, main effect of Injection/Delay: $F_{5,17} = 9.14$, $P < 0.001$) surrounding PV^+ interneurons (D, ANOVA, main effect of Injection/Delay: $F_{5,17} = 9.58$, $P < 0.001$) at 3-7dpi, with eventual regeneration of PNNs occurring by 14-28 dpi. ChABC treatment did not alter PV^+ interneuron density (E, ANOVA, $P > 0.05$), but loss of PNNs led to a retraction of PV^+ neurites in the pyramidal cell layer (F, unpaired *t*-test: $t_6 = 6.37$, $P < 0.001$). **(G to L)** Adult mice were microinjected with Penicillinase or ChABC at different time points before contextual fear conditioning (G). ChABC treatment did not alter freezing behavior during training (H, ANOVA, $P > 0.05$) but reduced memory precision at 3- (I, ANOVA, Injection

× Test Context interaction: $F_{1,24}$ = 20.40, P < 0.001) and 7-dpi (J, ANOVA, Injection × Test Context interaction: $F_{1,28}$ = 9.64, P < 0.01) when PNNs levels remained low. Adult-like memory precision was restored once PNN levels recovered at 14- (K, ANOVA, main effect of Test Context: $F_{1,27}$ = 74.82, $P < 10^{-6}$) and 28-dpi (L, ANOVA, main effect of Test Context: $F_{1,20}$ = 68.26, $P < 10^{-6}$). **(M)** PNN digestion with ChABC did not reduce precision for short-term (1 h) memories (ANOVA, main effect of Injection: $F_{1,28}$ = 5.46, P < 0.05; main effect of Test Context: $F_{1,28}$ = 90.74, $P < 10^{-6}$). **(N to R)** Microinjection of ChABC into dorsal CA1 of adult mice before an open field and elevated-plus maze exploration (N), did not alter anxiety-like behavior or locomotion in the open field (O, unpaired *t*-test: t_{10} = 0.11, P = 0.91; P, unpaired *t*-test: t_{10} = 0.69, P = 0.50) or on the elevated-plus maze (Q, unpaired *t*-test: t_{10} = 0.31, P = 0.76; R, unpaired *t*-test: t_{10} = 0.27, P = 0.79). Data points are individual mice with mean ± s.e.m. Scale bars: white = 50 μm, yellow = 500 μm. * P < 0.05; ** P < 0.01; *** P < 0.001.

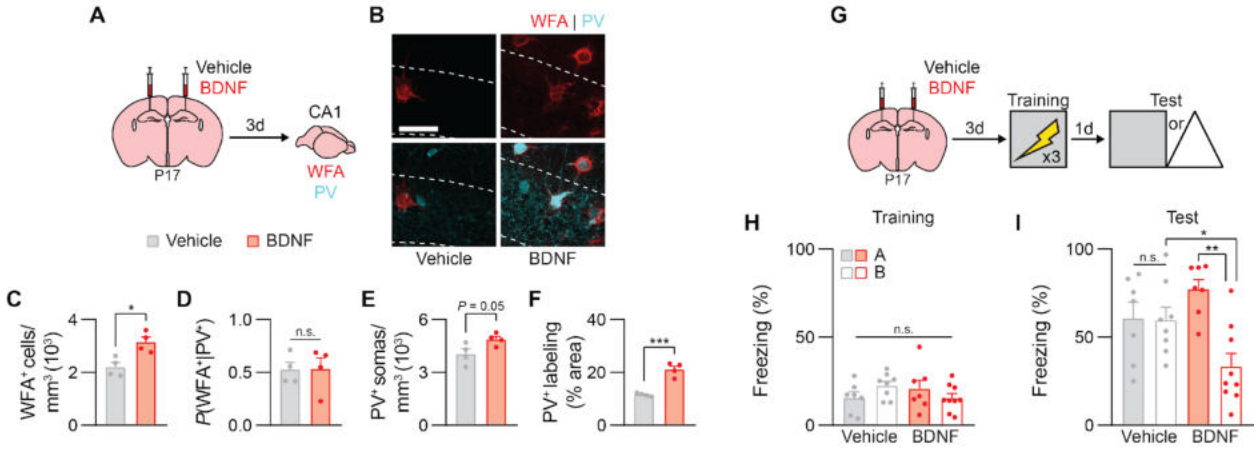

Figure S18. Accelerating CA1 PNN development with BDNF results in early onset of adult-like memory precision. (A to B) Recombinant BDNF protein was microinjected into the dorsal CA1 of juvenile mice (A) to promote PNN maturation (B). **(C to F)** BDNF treatment increased the density of WFA^+ PNNs in the P20 CA1 (C, unpaired *t*-test: $t_6 = 3.64$, $P < 0.05$). The proportion of PV^+ interneurons surrounded by WFA^+ PNNs was not increased (D, unpaired *t*-test: $t_6 = 0.051$, $P = 0.96$), as BDNF also increased the number of PV^+ interneurons (E, unpaired *t*-test: $t_6 = 2.42$, $P = 0.05$) and density of PV^+ neurites (F, unpaired *t*-test: $t_6 = 7.14$, $P < 0.001$) in P20 CA1. **(G to I)** Juvenile mice were microinjected with Vehicle or BDNF 3 days before contextual fear conditioning (G). BDNF treatment did not alter freezing behavior during training (H, ANOVA, $P > 0.05$) but improved memory precision during the test (I, ANOVA, Injection × Test Context interaction: $F_{1,27} = 8.04$, $P < 0.01$). Data points are individual mice with mean ± s.e.m. Scale bars: white = 50 μm. * $P < 0.05$; ** $P < 0.01$.

References and Notes

1. C. T. Ngo, Y. Lin, N. S. Newcombe, I. R. Olson, Building up and wearing down episodic memory: Mnemonic discrimination and relational binding. *J. Exp. Psychol. Gen.* **148**, 1463–1479 (2019). doi:10.1037/xge0000583 Medline

2. L. Picard, S. Cousin, B. Guillery-Girard, F. Eustache, P. Piolino, How do the different components of episodic memory develop? Role of executive functions and short-term feature-binding abilities. *Child Dev.* **83**, 1037–1050 (2012). doi:10.1111/j.1467-8624.2012.01736.x Medline

3. H. Yim, A. F. Osth, V. M. Sloutsky, S. J. Dennis, Sources of interference in memory across development. *Psychol. Sci.* **33**, 1154–1171 (2022). doi:10.1177/09567976211073131 Medline

4. L. Rollins, E. B. Cloude, Development of mnemonic discrimination during childhood. *Learn. Mem.* **25**, 294–297 (2018). doi:10.1101/lm.047142.117 Medline

5. J. Bachevalier, F. Vargha-Khadem, The primate hippocampus: Ontogeny, early insult and memory. *Curr. Opin. Neurobiol.* **15**, 168–174 (2005). doi:10.1016/j.conb.2005.03.015 Medline

6. R. Cossart, R. Khazipov, How development sculpts hippocampal circuits and function. *Physiol. Rev.* **102**, 343–378 (2022). doi:10.1152/physrev.00044.2020 Medline

7. A. Keresztes, C. T. Ngo, U. Lindenberger, M. Werkle-Bergner, N. S. Newcombe, hippocampal maturation drives memory from generalization to specificity. *Trends Cogn. Sci.* **22**, 676–686 (2018). doi:10.1016/j.tics.2018.05.004 Medline

8. A. I. Ramsaran, M. L. Schlichting, P. W. Frankland, The ontogeny of memory persistence and specificity. *Dev. Cogn. Neurosci.* **36**, 100591 (2019). doi:10.1016/j.dcn.2018.09.002 Medline

9. T. A. Allen, N. J. Fortin, The evolution of episodic memory. *Proc. Natl. Acad. Sci. U.S.A.* **110** (Suppl 2), 10379–10386 (2013). doi:10.1073/pnas.1301199110 Medline

10. M. J. Anderson, D. C. Riccio, Ontogenetic forgetting of stimulus attributes. *Learn. Behav.* **33**, 444–453 (2005). doi:10.3758/BF03193183 Medline

11. I. Goshen, M. Brodsky, R. Prakash, J. Wallace, V. Gradinaru, C. Ramakrishnan, K. Deisseroth, Dynamics of retrieval strategies for remote memories. *Cell* **147**, 678–689 (2011). doi:10.1016/j.cell.2011.09.033 Medline

12. L. Nadel, S. Zola-Morgan, "Infantile amnesia," in *Infant Memory*, M. Moscovitch, Ed. (Springer, 1984), vol. 9, pp. 145–172.

13. J. Bachevalier, M. Mishkin, An early and a late developing system for learning and retention in infant monkeys. *Behav. Neurosci.* **98**, 770–778 (1984). doi:10.1037/0735-7044.98.5.770 Medline

14. C. T. Ellis, L. J. Skalaban, T. S. Yates, V. R. Bejjanki, N. I. Córdova, N. B. Turk-Browne, Evidence of hippocampal learning in human infants. *Curr. Biol.* **31**, 3358–3364.e4 (2021). doi:10.1016/j.cub.2021.04.072 Medline

15. A. C. Schapiro, N. B. Turk-Browne, M. M. Botvinick, K. A. Norman, Complementary learning systems within the hippocampus: A neural network modelling approach to

reconciling episodic memory with statistical learning. *Philos. Trans. R. Soc. Lond. B Biol. Sci.* **372**, 20160049 (2017). doi:10.1098/rstb.2016.0049 Medline

16. S. A. Josselyn, S. Köhler, P. W. Frankland, Finding the engram. *Nat. Rev. Neurosci.* **16**, 521–534 (2015). doi:10.1038/nrn4000 Medline

17. J. T. Wixted, L. R. Squire, Y. Jang, M. H. Papesh, S. D. Goldinger, J. R. Kuhn, K. A. Smith, D. M. Treiman, P. N. Steinmetz, Sparse and distributed coding of episodic memory in neurons of the human hippocampus. *Proc. Natl. Acad. Sci. U.S.A.* **111**, 9621–9626 (2014). doi:10.1073/pnas.1408365111 Medline

18. K. Z. Tanaka, H. He, A. Tomar, K. Niisato, A. J. Y. Huang, T. J. McHugh, The hippocampal engram maps experience but not place. *Science* **361**, 392–397 (2018). doi:10.1126/science.aat5397 Medline

19. K. K. Tayler, K. Z. Tanaka, L. G. Reijmers, B. J. Wiltgen, Reactivation of neural ensembles during the retrieval of recent and remote memory. *Curr. Biol.* **23**, 99–106 (2013). doi:10.1016/j.cub.2012.11.019 Medline

20. D. J. Cai, D. Aharoni, T. Shuman, J. Shobe, J. Biane, W. Song, B. Wei, M. Veshkini, M. La-Vu, J. Lou, S. E. Flores, I. Kim, Y. Sano, M. Zhou, K. Baumgaertel, A. Lavi, M. Kamata, M. Tuszynski, M. Mayford, P. Golshani, A. J. Silva, A shared neural ensemble links distinct contextual memories encoded close in time. *Nature* **534**, 115–118 (2016). doi:10.1038/nature17955 Medline

21. F. Donato, R. I. Jacobsen, M.-B. Moser, E. I. Moser, Stellate cells drive maturation of the entorhinal-hippocampal circuit. *Science* **355**, eaai8178 (2017). doi:10.1126/science.aai8178 Medline

22. A. Travaglia, R. Bisaz, E. Cruz, C. M. Alberini, Developmental changes in plasticity, synaptic, glia and connectivity protein levels in rat dorsal hippocampus. *Neurobiol. Learn. Mem.* **135**, 125–138 (2016). doi:10.1016/j.nlm.2016.08.005 Medline

23. X. Gao, S. Castro-Gomez, J. Grendel, S. Graf, U. Süsens, L. Binkle, D. Mensching, D. Isbrandt, D. Kuhl, O. Ohana, Arc/Arg3.1 mediates a critical period for spatial learning and hippocampal networks. *Proc. Natl. Acad. Sci. U.S.A.* **115**, 12531–12536 (2018). doi:10.1073/pnas.1810125115 Medline

24. S. G. Leinwand, K. Scott, Juvenile hormone drives the maturation of spontaneous mushroom body neural activity and learned behavior. *Neuron* **109**, 1836–1847.e5 (2021). doi:10.1016/j.neuron.2021.04.006 Medline

25. S. A. Josselyn, P. W. Frankland, Memory allocation: Mechanisms and function. *Annu. Rev. Neurosci.* **41**, 389–413 (2018). doi:10.1146/annurev-neuro-080317-061956 Medline

26. A. J. Rashid, C. Yan, V. Mercaldo, H.-L. L. Hsiang, S. Park, C. J. Cole, A. De Cristofaro, J. Yu, C. Ramakrishnan, S. Y. Lee, K. Deisseroth, P. W. Frankland, S. A. Josselyn, Competition between engrams influences fear memory formation and recall. *Science* **353**, 383–387 (2016). doi:10.1126/science.aaf0594 Medline

27. D. J. Morrison, A. J. Rashid, A. P. Yiu, C. Yan, P. W. Frankland, S. A. Josselyn, Parvalbumin interneurons constrain the size of the lateral amygdala engram. *Neurobiol. Learn. Mem.* **135**, 91–99 (2016). doi:10.1016/j.nlm.2016.07.007 Medline

28. F. Donato, A. Chowdhury, M. Lahr, P. Caroni, Early- and late-born parvalbumin basket cell subpopulations exhibiting distinct regulation and roles in learning. *Neuron* **85**, 770–786 (2015). doi:10.1016/j.neuron.2015.01.011 Medline

29. D. Doischer, J. A. Hosp, Y. Yanagawa, K. Obata, P. Jonas, I. Vida, M. Bartos, Postnatal differentiation of basket cells from slow to fast signaling devices. *J. Neurosci.* **28**, 12956–12968 (2008). doi:10.1523/JNEUROSCI.2890-08.2008 Medline

30. L. Que, D. Lukacsovich, W. Luo, C. Földy, Transcriptional and morphological profiling of parvalbumin interneuron subpopulations in the mouse hippocampus. *Nat. Commun.* **12**, 108 (2021). doi:10.1038/s41467-020-20328-4 Medline

31. T. K. Hensch, Critical period plasticity in local cortical circuits. *Nat. Rev. Neurosci.* **6**, 877–888 (2005). doi:10.1038/nrn1787 Medline

32. Z. J. Huang, A. Kirkwood, T. Pizzorusso, V. Porciatti, B. Morales, M. F. Bear, L. Maffei, S. Tonegawa, BDNF regulates the maturation of inhibition and the critical period of plasticity in mouse visual cortex. *Cell* **98**, 739–755 (1999). doi:10.1016/S0092-8674(00)81509-3 Medline

33. E. Dzyubenko, M. Fleischer, D. Manrique-Castano, M. Borbor, C. Kleinschnitz, A. Faissner, D. M. Hermann, Inhibitory control in neuronal networks relies on the extracellular matrix integrity. *Cell. Mol. Life Sci.* **78**, 5647–5663 (2021). doi:10.1007/s00018-021-03861-3 Medline

34. E. Favuzzi, A. Marques-Smith, R. Deogracias, C. M. Winterflood, A. Sánchez-Aguilera, L. Mantoan, P. Maeso, C. Fernandes, H. Ewers, B. Rico, Activity-dependent gating of parvalbumin interneuron function by the perineuronal net protein brevican. *Neuron* **95**, 639–655.e10 (2017). doi:10.1016/j.neuron.2017.06.028 Medline

35. T. Pizzorusso, P. Medini, N. Berardi, S. Chierzi, J. W. Fawcett, L. Maffei, Reactivation of ocular dominance plasticity in the adult visual cortex. *Science* **298**, 1248–1251 (2002). doi:10.1126/science.1072699 Medline

36. J. W. Fawcett, T. Oohashi, T. Pizzorusso, The roles of perineuronal nets and the perinodal extracellular matrix in neuronal function. *Nat. Rev. Neurosci.* **20**, 451–465 (2019). doi:10.1038/s41583-019-0196-3 Medline

37. O. Senkov, P. Andjus, L. Radenovic, E. Soriano, A. Dityatev, Neural ECM molecules in synaptic plasticity, learning, and memory. *Prog. Brain Res.* **214**, 53–80 (2014). doi:10.1016/B978-0-444-63486-3.00003-7 Medline

38. V. Nagy, O. Bozdagi, A. Matynia, M. Balcerzyk, P. Okulski, J. Dzwonek, R. M. Costa, A. J. Silva, L. Kaczmarek, G. W. Huntley, Matrix metalloproteinase-9 is required for hippocampal late-phase long-term potentiation and memory. *J. Neurosci.* **26**, 1923–1934 (2006). doi:10.1523/JNEUROSCI.4359-05.2006 Medline

39. D. Carulli, T. Pizzorusso, J. C. F. Kwok, E. Putignano, A. Poli, S. Forostyak, M. R. Andrews, S. S. Deepa, T. T. Glant, J. W. Fawcett, Animals lacking link protein have attenuated perineuronal nets and persistent plasticity. *Brain* **133**, 2331–2347 (2010). doi:10.1093/brain/awq145 Medline

40. K. Matsumoto, M. Shionyu, M. Go, K. Shimizu, T. Shinomura, K. Kimata, H. Watanabe, Distinct interaction of versican/PG-M with hyaluronan and link protein. *J. Biol. Chem.* **278**, 41205–41212 (2003). doi:10.1074/jbc.M305060200 Medline

41. U. Farooq, G. Dragoi, Emergence of preconfigured and plastic time-compressed sequences in early postnatal development. *Science* **363**, 168–173 (2019). doi:10.1126/science.aav0502 Medline

42. A. Figurov, L. D. Pozzo-Miller, P. Olafsson, T. Wang, B. Lu, Regulation of synaptic responses to high-frequency stimulation and LTP by neurotrophins in the hippocampus. *Nature* **381**, 706–709 (1996). doi:10.1038/381706a0 Medline

43. Y. Jeong, H.-Y. Cho, M. Kim, J.-P. Oh, M. S. Kang, M. Yoo, H.-S. Lee, J.-H. Han, Synaptic plasticity-dependent competition rule influences memory formation. *Nat. Commun.* **12**, 3915 (2021). doi:10.1038/s41467-021-24269-4 Medline

44. H. Norimoto, K. Makino, M. Gao, Y. Shikano, K. Okamoto, T. Ishikawa, T. Sasaki, H. Hioki, S. Fujisawa, Y. Ikegaya, Hippocampal ripples down-regulate synapses. *Science* **359**, 1524–1527 (2018). doi:10.1126/science.aao0702 Medline

45. A. K. Saghatelyan, S. Gorissen, M. Albert, B. Hertlein, M. Schachner, A. Dityatev, The extracellular matrix molecule tenascin-R and its HNK-1 carbohydrate modulate perisomatic inhibition and long-term potentiation in the CA1 region of the hippocampus. *Eur. J. Neurosci.* **12**, 3331–3342 (2000). doi:10.1046/j.1460-9568.2000.00216.x Medline

46. M. T. Birnie, T. Z. Baram, Principles of emotional brain circuit maturation. *Science* **376**, 1055–1056 (2022). doi:10.1126/science.abn4016 Medline

47. E. M. Nabel, H. Morishita, Regulating critical period plasticity: Insight from the visual system to fear circuitry for therapeutic interventions. *Front. Psychiatry* **4**, 146 (2013). doi:10.3389/fpsyt.2013.00146 Medline

48. N. Gogolla, P. Caroni, A. Lüthi, C. Herry, Perineuronal nets protect fear memories from erasure. *Science* **325**, 1258–1261 (2009). doi:10.1126/science.1174146 Medline

49. R. V. Kail, N. E. Spear, "Ecologically determined dispositions control the ontogeny of learning and memory," in *Comparative Perspectives on the Development of Memory*, R. V. Kail, N. E. Spear, Eds. (Psychology Press, 1984); pp. 325–358.

50. A. Gopnik, Childhood as a solution to explore-exploit tensions. *Philos. Trans. R. Soc. Lond. B Biol. Sci.* **375**, 20190502 (2020). doi:10.1098/rstb.2019.0502 Medline

51. A. Ramsaran, Y. Wang, A. Golbabaei, S. Aleshin, M. L. de Snoo, B. A. Yeung, A. J. Rashid, A. Awasthi, J. Lau, L. M. Tran, S. Y. Ko, A. Abegg, L. Chunan Duan, C. McKenzie, J. Gallucci, M. Ahmed, R. Kaushik, A. Dityatev, S. A. Josselyn, P. W. Frankland, Data for: A shift in the mechanisms controlling hippocampal engram formation during brain maturation, Dryad (2023); https://doi.org/10.5061/dryad.w3r2280w4.

52. T. S. Doherty, J. Blaze, S. M. Keller, T. L. Roth, Phenotypic outcomes in adolescence and adulthood in the scarcity-adversity model of low nesting resources outside the home cage. *Dev. Psychobiol.* **59**, 703–714 (2017). doi:10.1002/dev.21547 Medline

53. S. Hippenmeyer, E. Vrieseling, M. Sigrist, T. Portmann, C. Laengle, D. R. Ladle, S. Arber, A developmental switch in the response of DRG neurons to ETS transcription factor signaling. *PLOS Biol.* **3**, e159 (2005). doi:10.1371/journal.pbio.0030159 Medline

54. T. Suzuki, S. Arai, M. Takeuchi, C. Sakurai, H. Ebana, T. Higashi, H. Hashimoto, K. Hatsuzawa, I. Wada, Development of cysteine-free fluorescent proteins for the oxidative environment. *PLOS ONE* **7**, e37551 (2012). doi:10.1371/journal.pone.0037551 Medline

55. A. P. Yiu, V. Mercaldo, C. Yan, B. Richards, A. J. Rashid, H.-L. L. Hsiang, J. Pressey, V. Mahadevan, M. M. Tran, S. A. Kushner, M. A. Woodin, P. W. Frankland, S. A. Josselyn, Neurons are recruited to a memory trace based on relative neuronal excitability immediately before training. *Neuron* **83**, 722–735 (2014). doi:10.1016/j.neuron.2014.07.017 Medline

56. S. J. Russo, M. B. Wilkinson, M. S. Mazei-Robison, D. M. Dietz, I. Maze, V. Krishnan, W. Renthal, A. Graham, S. G. Birnbaum, T. A. Green, B. Robison, A. Lesselyong, L. I. Perrotti, C. A. Bolaños, A. Kumar, M. S. Clark, J. F. Neumaier, R. L. Neve, A. L. Bhakar, P. A. Barker, E. J. Nestler, Nuclear factor κ B signaling regulates neuronal morphology and cocaine reward. *J. Neurosci.* **29**, 3529–3537 (2009). doi:10.1523/JNEUROSCI.6173-08.2009 Medline

57. A. Travaglia, R. Bisaz, E. S. Sweet, R. D. Blitzer, C. M. Alberini, Infantile amnesia reflects a developmental critical period for hippocampal learning. *Nat. Neurosci.* **19**, 1225–1233 (2016). doi:10.1038/nn.4348 Medline

58. M. Arruda-Carvalho, W.-C. Wu, K. A. Cummings, R. L. Clem, Optogenetic examination of prefrontal-amygdala synaptic development. *J. Neurosci.* **37**, 2976–2985 (2017). doi:10.1523/JNEUROSCI.3097-16.2017 Medline

59. A. I. Ramsaran, S. R. Westbrook, M. E. Stanton, Ontogeny of object-in-context recognition in the rat. *Behav. Brain Res.* **298** (Pt A), 37–47 (2016). doi:10.1016/j.bbr.2015.04.011 Medline

60. J. Olds, P. Milner, Positive reinforcement produced by electrical stimulation of septal area and other regions of rat brain. *J. Comp. Physiol. Psychol.* **47**, 419–427 (1954). doi:10.1037/h0058775 Medline

61. M. S. Fanselow, Conditioned and unconditional components of post-shock freezing. *Pavlov. J. Biol. Sci.* **15**, 177–182 (1980). doi:10.1007/BF03001163 Medline

62. A. Asok, J. Hijazi, L. R. Harvey, S. Kosmidis, E. R. Kandel, J. B. Rayman, Sex differences in remote contextual fear generalization in mice. *Front. Behav. Neurosci.* **13**, 56 (2019). doi:10.3389/fnbeh.2019.00056 Medline

63. J. C. Biedenkapp, J. W. Rudy, Context preexposure prevents forgetting of a contextual fear memory: Implication for regional changes in brain activation patterns associated with recent and remote memory tests. *Learn. Mem.* **14**, 200–203 (2007). doi:10.1101/lm.499407 Medline

64. T. J. Ryan, D. S. Roy, M. Pignatelli, A. Arons, S. Tonegawa, Memory. Engram cells retain memory under retrograde amnesia. *Science* **348**, 1007–1013 (2015). doi:10.1126/science.aaa5542 Medline

65. R. G. Morris, P. Garrud, J. N. P. Rawlins, J. O'Keefe, Place navigation impaired in rats with hippocampal lesions. *Nature* **297**, 681–683 (1982). doi:10.1038/297681a0 Medline

66. T. Feng, C. Alicea, V. Pham, A. Kirk, S. Pieraut, Experience-dependent inhibitory plasticity is mediated by CCK+ basket cells in the developing dentate gyrus. *J. Neurosci.* **41**, 4607–4619 (2021). doi:10.1523/JNEUROSCI.1207-20.2021 Medline

67. R. F. Dard, E. Leprince, J. Denis, S. Rao Balappa, D. Suchkov, R. Boyce, C. Lopez, M. Giorgi-Kurz, T. Szwagier, T. Dumont, H. Rouault, M. Minlebaev, A. Baude, R. Cossart, M. A. Picardo, The rapid developmental rise of somatic inhibition disengages hippocampal dynamics from self-motion. *eLife* **11**, e78116 (2022). doi:10.7554/eLife.78116 Medline

68. S. Trouche, J. M. Sasaki, T. Tu, L. G. Reijmers, Fear extinction causes target-specific remodeling of perisomatic inhibitory synapses. *Neuron* **80**, 1054–1065 (2013). doi:10.1016/j.neuron.2013.07.047 Medline

69. P. Davis, Y. Zaki, J. Maguire, L. G. Reijmers, Cellular and oscillatory substrates of fear extinction learning. *Nat. Neurosci.* **20**, 1624–1633 (2017). doi:10.1038/nn.4651 Medline

70. C. I. Seidenbecher, K. Richter, U. Rauch, R. Fässler, C. C. Garner, E. D. Gundelfinger, Brevican, a chondroitin sulfate proteoglycan of rat brain, occurs as secreted and cell surface glycosylphosphatidylinositol-anchored isoforms. *J. Biol. Chem.* **270**, 27206–27212 (1995). doi:10.1074/jbc.270.45.27206 Medline